

UrbanFM: Scaling Urban Spatio-Temporal Foundation Models

Wei Chen^{1,2}, Yuqian Wu², Junle Chen¹, Xiaofang Zhou^{1*}, Yuxuan Liang^{2*}

¹HKUST, ²HKUST(GZ)

Urban systems, as dynamic complex systems, continuously generate spatio-temporal data streams that encode the fundamental laws of human mobility and city evolution. While AI for Science has witnessed the transformative power of foundation models in disciplines like genomics and meteorology, urban computing remains fragmented due to “scenario-specific” models, which are overfitted to specific regions or tasks, hindering their generalizability. To bridge this gap and advance spatio-temporal foundation models for urban systems, we adopt scaling as the central perspective and systematically investigate two key questions: what to scale and how to scale. Grounded in first-principles analysis, we identify three critical dimensions: **heterogeneity**, **correlation**, and **dynamics**, aligning these principles with the fundamental scientific properties of urban spatio-temporal data. Specifically, to address heterogeneity through **data scaling**, we construct WorldST. This billion-scale corpus standardizes diverse physical signals, such as traffic flow and speed, from over 100 global cities into a unified data format. To enable **computation scaling** for modeling correlations, we introduce the MiniST unit, a novel split mechanism that discretizes continuous spatio-temporal fields into learnable computational units to unify representations of grid-based and sensor-based observations. Finally, addressing dynamics via **architecture scaling**, we propose UrbanFM, a minimalist self-attention architecture designed with limited inductive biases to autonomously learn dynamic spatio-temporal dependencies from massive data. Furthermore, to ensure fair evaluation, we establish EvalST, the largest-scale urban spatio-temporal benchmark to date. Extensive experiments demonstrate that UrbanFM achieves remarkable zero-shot generalization across unseen cities and tasks, marking a pivotal first step toward large-scale pretrained urban spatio-temporal foundation models.

Correspondence: onedeanxxx@gmail.com

Date: Feb 9, 2026

1 Introduction

Modern cities (Dong et al., 2024), functioning as dynamically evolving complex systems, continuously generate multi-source spatio-temporal data streams, encompassing a wide range of mobility information, from traffic flow to population movement. These ubiquitous data streams constantly depict the dynamic pulse of urban systems, encoding the fundamental scientific laws governing urban evolution (Pappalardo et al., 2023).

Over the past two decade, statistical methods (Cressie and Wikle, 2011) and spatio-temporal deep neural networks (Jin et al., 2023) have achieved success in specific urban tasks like traffic forecasting (Jin et al., 2024) and imputation (Gao et al., 2022). However, these methods face the dilemma of “scenario customization”: most models (Marisca et al., 2024; Nie et al., 2024; Cini et al., 2022; Li et al., 2018) are optimized for single urban regions, specific time spans, or isolated scenarios, lacking universal modeling capabilities for general characteristics of urban systems.

Reflecting on technological history, the “bitter lesson” (Sutton, 2019) reveals that when computational scale surpasses critical thresholds, general-purpose paradigms leveraging massive data inevitably outperform complex human-designed heuristics. Although recent foundation models have achieved knowledge compression through scaling (Kaplan et al., 2020) and demonstrated remarkable generalization capabilities in language (Brown et al., 2020) and vision (Hurst et al., 2024) domains, as illustrated in Figure 1 top, the scaling of spatio-temporal knowledge and intelligence for urban systems is still impeded by three fundamental scientific barriers:

Challenge I. Heterogeneity: Tobler’s Second Law (Tobler, 1970) of Geography reveals that urban data exhibits

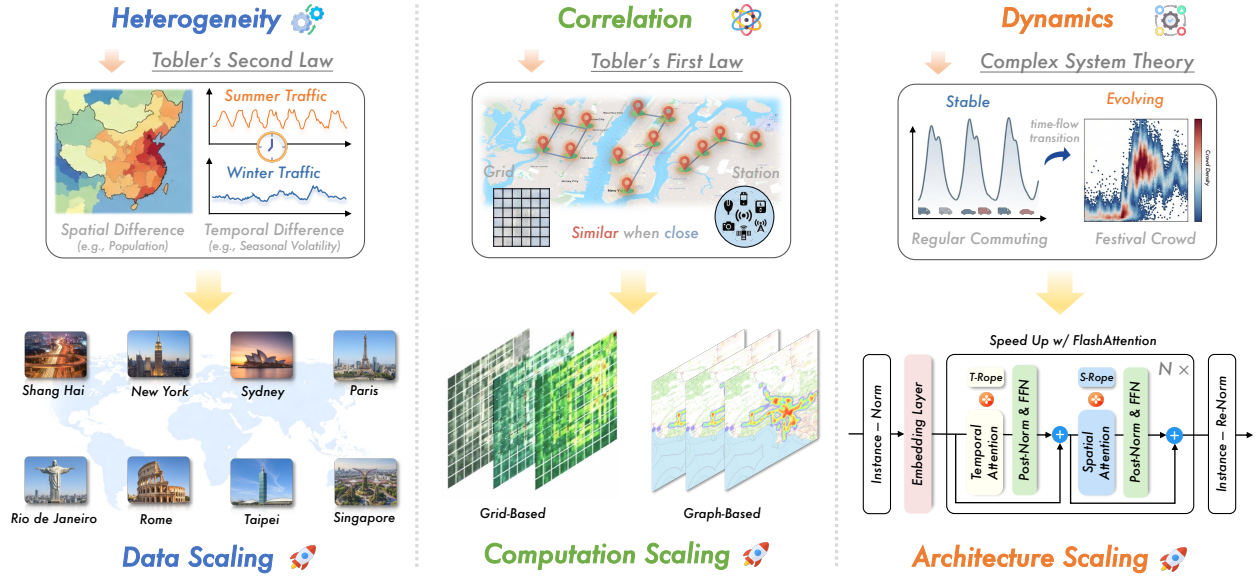


Figure 1 Top: The fundamental nature of spatio-temporal data and challenges of urban ST foundational models. Bottom: Three core perspectives of scaling the urban ST foundation model: data, computation, and architecture.

significant spatio-temporal heterogeneity across domains. Specifically, the characteristics or relations of variables differ markedly across varying spatial locations or temporal points. This heterogeneity manifests as inherent non-uniformity and complexity, exemplified by spatial variances such as population density differences or temporal fluctuations like seasonal traffic volatility. Consequently, achieving *data scaling*, which involves aggregating massive amounts of multi-source heterogeneous urban data to comprehensively cover the true distribution, serves as the fundamental solution to addressing heterogeneity.

Challenge II. Correlation: Tobler’s First Law (Tobler, 1970) of Geography dictates that urban data possesses high spatio-temporal autocorrelation, meaning that attributes are interrelated across time and space, with proximity strengthening these associations. However, modeling these dependencies is further complicated by the coexistence of diverse microscopic and macroscopic data types (e.g., grid-based macro mobility patterns versus station-based micro sensor observations (Wang et al., 2020)). Therefore, achieving *computation scaling*, by leveraging these spatio-temporal autocorrelations to segment data into unified and appropriate computational units, constitutes the primary means to resolve the challenge of spatio-temporal correlation.

Challenge III. Dynamics: Complex System Theory (Thurner et al., 2018) posits that urban systems are inherently non-stationary. Interactions between entities evolve continuously over time rather than remaining static, as exemplified by the stark contrast between regular commuting flows and irregular festival crowd dynamics. Existing architectures often inject strong inductive biases, such as static graph structures, which fail to capture these shifting patterns. Thus, achieving *architecture scaling*, by designing minimalist architectures with limited inductive biases to autonomously learn time-evolving dependencies, represents the real challenge to mastering system dynamics.

To systematically address these challenges, as illustrated in Figure 1 bottom, we design scalable, principled components tailored to distinct scientific properties. Our contributions are summarized as follows:

- *Data Scaling:* We construct the **WorldST**, employing a rigorous standardization pipeline to normalize heterogeneous signals from over 100 global cities into a unified data format, thereby ensuring distributional compatibility.
- *Computation Scaling:* We develop **MiniST**, a novel split mechanism that transforms disparate grid and sensor inputs into unified learnable units, enabling the scalable computation of spatio-temporal correlations.
- *Architecture Scaling:* We design **UrbanFM**, a minimalist adaptation of the self-attention architecture intended to minimize manual priors, which empowers the model to autonomously capture complex dynamic patterns.

- Additionally, we establish EvalST, the largest spatio-temporal evaluation benchmark to date. Experimental results demonstrate that UrbanFM achieves remarkable zero-shot generalization in all tasks. We regard this work as a pivotal advancement toward large-scale spatio-temporal foundation models in urban science.

2 Related Work

2.0.1 Spatio-Temporal Data Science

Spatio-temporal data science focuses on modeling the temporal evolution of spatially distributed variables, where forecasting and imputation constitute two fundamental tasks (Liang et al., 2025; Chen et al., 2024b). These problems are central to a wide range of urban applications, including traffic management (Ermagun and Levinson, 2018), environmental monitoring (Dietze et al., 2024), and public safety (Wu et al., 2025c,b). Early studies predominantly relied on statistical and classical machine learning approaches (Shi and Yeung, 2018), such as ARIMA (Box and Pierce, 1970), VAR (Biller and Nelson, 2003), and Gaussian Processes (Hamelijnck et al., 2021), which explicitly model temporal dependencies but scale poorly to large, heterogeneous urban systems. With the advent of deep learning, spatio-temporal neural models (Shao et al., 2024; Chen et al., 2025) have become the prevailing paradigm, typically integrating temporal sequence modeling with spatial dependency learning. Representative architectures include CNN-based models (Wang et al., 2020; Zhang et al., 2017; Liu et al., 2020) for capturing local spatial correlations, RNN- (Li et al., 2018; Wang et al., 2022) or Transformer-based (Guo et al., 2019; Liu et al., 2023) models for temporal dynamics, and graph neural networks (Wu et al., 2019; Song et al., 2020; Shao et al., 2022b; Han et al., 2024; Ma et al., 2025) for explicitly encoding non-Euclidean spatial structures such as road networks or sensor graphs. Recent advances emphasize unified representation learning, with spatio-temporal graph neural networks (Jin et al., 2023, 2024) serving as a prominent example. Despite strong empirical performance, most existing approaches remain task-specific and dataset-dependent, often requiring architectural modifications or retraining (Chen and Liang, 2025a,b) when transferred across domains, cities, or temporal horizons. *These limitations motivate the exploration of more generalizable paradigms that move beyond single-task modeling toward reusable spatio-temporal models.*

2.0.2 Urban Foundation Models

Inspired by the success of foundation models (Chen et al., 2024a) in language (Brown et al., 2020) and vision (Hurst et al., 2024) domains, Urban Foundation Models (Zhang et al., 2024), also termed Spatio-Temporal Foundation Models (Fang et al., 2026), aim to learn general-purpose representations from large-scale, heterogeneous urban data to efficiently adapt to diverse downstream tasks. Early research typically employed self-supervised pre-training with pretext tasks, such as contrastive learning (Qu et al., 2022; Zheng et al., 2024) or masked auto-encoding (Gao et al., 2024; Liu and Zhang, 2025), to learn general representations. However, these methods were generally confined to single cities or domains, lacking cross-city zero-shot transferability. With the emergence of the foundation model paradigm, recent studies (Yuan et al., 2024a,b) have shifted towards jointly training shared spatio-temporal encoders on multi-city datasets, demonstrating enhanced capabilities for cross-city transfer forecasting. Subsequent research has further explored the efficacy of diverse backbones, including vanilla Transformers (Han et al., 2025), Diffusion Transformers (Yuan et al., 2025), Graph Conventional Models (Li et al., 2025), Mixture-of-Experts (Tang et al., 2025), and State Space Models (An et al., 2026), while often incorporating external augmentations such as frozen Language Models (Yu et al., 2025; Liu et al., 2025b). Although recent strategies (Zhong et al., 2025, 2026) further advocate for disentangling spatial and temporal components within the “pre-training & fine-tuning” paradigm, the field remains predominantly focused on architectural novelty. *In contrast, we revisit the fundamental scientific properties of urban spatio-temporal data and propose a principled multi-dimensional scaling approach to unlock authentic zero-shot generalization.*

3 Preliminary

Definition 1 (Urban Spatio-temporal Data). Spatio-temporal data describes the continuous observational data that varies over time at different spatial locations in a city. It is uniformly represented as a third-order

tensor $\mathbf{X} \in \mathbb{R}^{N \times T \times C}$, where N denotes the number of spatial locations, T indicates the number of temporal recording steps, and C typically represents a single recorded element feature, including various spatio-temporal data in the city, such as traffic speed, road occupancy rate, crowd flows, taxi demand, bike usage, cellular traffic, and others. Along the temporal dimension, the data can be approximated as a continuously varying system with smooth transitions. However, due to the discrete nature of data collection, the spatial dimension is further divided into two types: (i). *Sensor-based Type*: This represents the changes in non-uniformly distributed spatial regions, recorded by N sensors. The spatial relationships can be explicitly constructed by the geographic coordinates (latitude and longitude) of these sensors, forming a topological graph that is represented as an adjacency matrix A . (ii). *Grid-based Type*: This represents the changes in uniformly distributed spatial regions, composed of N grid cells. In this case, the spatial relationships are implicitly expressed by reshaping the N regions into a $W \times H$ format.

Definition 2 (Urban Spatio-temporal Task). Based on these different data, urban spatio-temporal tasks are primarily categorized into the following two types:

- Forecasting: Given T_h historical time steps of spatio-temporal sample $X \in \mathbb{R}^{N \times T_h \times C}$, predict future signals \hat{Y} over T_f time steps. This task can be further divided into:
 - ▶ Short-term Forecasting: Where T_f is relatively small (e.g., $T_f \leq 12$, about 1 hour), focusing on near-future predictions.
 - ▶ Long-term Forecasting: Where T_f is larger (e.g., $T_f > 12$, more than 1 hour), capturing extended trends.
- Imputation: Given an incomplete spatio-temporal sample $X \in \mathbb{R}^{N \times T \times C}$ with missing values indicated by a binary mask $M \in \{0, 1\}^{N \times T \times C}$, reconstruct the missing entries to obtain a complete dataset \hat{Y} . For each index (i, t, c) , we define $M_{i,t,c} = 1$ if $X_{i,t,c}$ is observed and $M_{i,t,c} = 0$ otherwise. This task can be divided into:
 - ▶ Point Imputation: For each discrete coordinate (i, t, c) satisfying $M_{i,t,c} = 0$, the task is to estimate the missing value $\hat{Y}_{i,t,c}$.
 - ▶ Block Imputation: For a contiguous set of indices $\mathcal{B} \subseteq \{(i, t, c)\}$ with $M_{i,t,c} = 0$ for all $(i, t, c) \in \mathcal{B}$, the block imputation aims to jointly recover all missing contiguous sub-tensor $\hat{\mathbf{Y}}_{\mathcal{B}}$.

Problem (Urban Spatio-temporal Foundation Models). Let the pre-training dataset be $\mathcal{D} = \{(X_i, Y_i)\}_{i=1}^{|\mathcal{D}|}$, where X_i represents urban spatio-temporal data (either grid-based or sensor-based) and Y_i denotes the corresponding target (future signals or imputed values). The goal is to train a foundational model f_θ that generalizes across different tasks \mathcal{T} (i.e., forecasting and imputation) and exhibits:

- Zero-shot: For an unseen dataset \mathcal{D}' , generate accurate predictions $\hat{Y}_i = f_\theta(X'_i)$ in any tasks without any datasets-specific examples.
- Few-shot: For an unseen dataset \mathcal{D}' , produce accurate predictions $\hat{Y}_i = f_\theta(X'_i)$ in any tasks with only a few labeled examples.

This foundation model needs to capture the knowledge of urban spatio-temporal data during pre-training, thereby achieving region and task-agnostic generalization for zero- and few-shot inference.

4 Methodology

We investigate scaling mechanisms from three perspectives: data, computation, and architecture. Data serves as the “fuel” for spatio-temporal knowledge and intelligence; computation defines the “tokenization” mechanism that transforms raw signals into learnable representations; architecture provides an “engine” with minimal inductive bias, designed to maximize scalability and transferability.

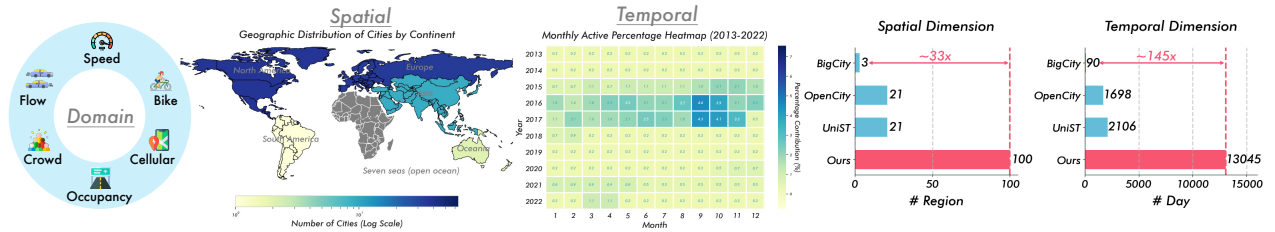


Figure 2 Data Overview: Breakthroughs in multi-domain coverage and spatio-temporal scale. Notably, we far surpass UniST (Yuan et al., 2024a), OpenCity (Li et al., 2025), and BigCity (Yu et al., 2025) in terms of spatial regions and temporal spans, by as much as 33 to 145 times.

4.1 Data Scaling

4.1.1 Intuition.

To effectively scale up urban spatio-temporal data, we need to consider two aspects: (i). *Domain Diversity*: Urban data should cover multiple domains to represent data sources from different physical systems and application categories (e.g., traffic, human, bicycle mobility, etc.). (ii). *Spatio-temporal Diversity*: The temporal dimension should cover multi-year changes, while the spatial dimension should encompass geographical patterns of global cities.

4.1.2 Solution.

Constructing a unified corpus from fragmented urban data silos requires a rigorous data curation pipeline. We propose a three-step protocol to aggregate, clean, and standardize heterogeneous data sources, resulting in a high-quality WorldST corpus, whose key characteristics are illustrated in Figure 2.

Step 1: Multi-Source Acquisition & Aggregation. To achieve the critical mass required for foundation models, we implemented a comprehensive data collection campaign targeting diverse urban areas. We aggregated raw data from two primary channels:

- *Open Government Portals*: We crawled archival data from municipal open data platforms (e.g., NYC Open Data¹, TfL Open Data², etc.). This provided massive-scale raw logs of public transit swipes, taxi trajectories, and bike-sharing records.
- *Established Academic Repositories*: We have also integrated some spatio-temporal datasets that have been open-sourced by academia (such as UCTB³, UTD-19⁴, etc.) to further enrich data diversity.
- *Domain-Specific APIs*: We accessed domain-specific APIs⁵ to retrieve fine-grained sensor readings, such as loop detector data for highway traffic speeds and occupancy rates.

Through this campaign, we curated a massive repository spanning 8 distinct domains (including Traffic Speed, Flow, Crow, etc.) across 100 cities globally. This raw collection encompasses over 1 billion data points, characterized by extreme heterogeneity in file formats (e.g., CSV, HDF5, NPZ, etc.) and metadata standards.

Step 2: Unified Ingestion & Alignment. The collected raw data exhibits significant inconsistency in storage formats and sampling frequencies. We developed a unified ingestion engine to standardize:

- *Format Unification*: We built adaptors to parse the diverse raw formats, mapping them into a standardized tensor $\mathbf{X}_{\text{raw}} \in \mathbb{R}^{N \times T \times C}$.

¹<https://opendata.cityofnewyork.us/>

²<https://tfl.gov.uk/info-for/open-data-users/our-open-data>

³<https://uctb.github.io/UCTB/index.html>

⁴<https://utd19.ethz.ch/>

⁵<https://pems.dot.ca.gov/>

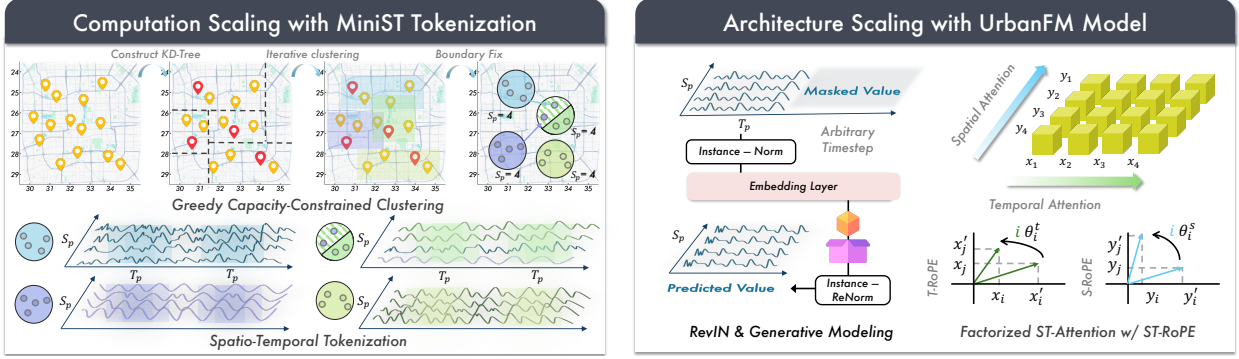


Figure 3 A schematic diagram of the scaling mechanism: MiniST tokenization and UrbanFM model.

- *Frequency Synchronization*: To address temporal heterogeneity, we standardized the time resolution to a base frequency Δt (i.e., 5 minutes). We apply *downsampling* via aggregation (sum/mean) for high-frequency streams and *linear interpolation* for low-frequency streams, ensuring temporal alignment across all cities.

Step 3: Quality Control & Pre-completion. Real-world sensors are prone to hardware failures (leading to missing values) and transmission errors (leading to noise). We implement a strict filtering and pre-completion mechanism to ensure data density:

- *Static Node Removal*: We calculate the variance σ_n^2 for each spatial node n . Nodes with $\sigma_n^2 \approx 0$ (indicating dead sensors or constant values) are discarded to prevent learning trivial mappings.
- *Outlier Clipping*: To mitigate the impact of extreme sensor noise, we apply the 3σ -rule. Values falling outside $[\mu - 3\sigma, \mu + 3\sigma]$ are treated as anomalies and replaced by boundary values.
- *Missing Value Pre-completion*: We ensure dense input tensor by pre-filling missing values. For small gaps, we use linear interpolation to reconstruct signal continuity. This ensures input tensors \mathbf{X} are complete and continuous, stabilizing learning.

4.1.3 Discussion.

Why this pipeline? Our pipeline prioritizes signal integrity and completeness. Simple concatenation of raw city datasets often introduces "poisonous" dead nodes or extensive gaps that destabilize foundation model training. By aggregating from diverse channels and enforcing strict quality control with temporal pre-completion, we transform fragmented urban logs into a consistent, dense "fuel" optimized for large-scale pre-training. Detailed information and data visualizations are provided in Appendix A.

4.2 Computation Scaling

4.2.1 Intuition.

Standard deep learning models necessitate fixed input dimensions for efficient parallelization; however, urban data exhibits inherent structural elasticity, with varying sensor counts and temporal spans across cities. To construct a foundation model, we require a generalized computational unit—analogue to “tokens” in NLP or “patches” in Vision Transformers—that decouples input size from model architecture while preserving the learnability of local spatio-temporal correlations. Specifically, urban systems manifest distinct correlation patterns: (i). *Temporal Order*: The natural sequential dependency (past influences future) must be strictly preserved. (ii). *Spatial Locality*: Spatial correlations are predominantly local but lack a natural 1D sequence. Consequently, the core challenge lies in: *How to efficiently partition continuous spatial fields into discrete, capacity-constrained units that maintain local proximity while enabling the model to learn spatial order as a sequence?*

4.2.2 Solution.

As shown in Figure 3 left, we introduce the MiniST

tokenization strategy, utilizing a dynamic split mechanism to transform heterogeneous urban data into unified input samples.

- *Greedy Capacity-Constrained Clustering*: Addressing the challenge of scalable topology modeling for varying N , we propose a spatially-aware grouping strategy inspired by KD-Tree logic (Samet, 2006), which partitions N spatial nodes into fixed-size clusters of size S_p to linearize spatial structures while preserving spatial relations.
 - ▶ We first construct a KD-Tree using geographic coordinates (latitude, longitude) of all sensors or grid cells (idx, idy).
 - ▶ We then iteratively query the tree to group the S_p nearest unassigned neighbors into a cluster. This ensures nodes within a token are geographically proximal, preserving local spatial correlations within the embedding itself.
 - ▶ For clusters with fewer than S_p nodes (boundary cases), we apply binary masking to maintain tensor uniformity.
- *Spatio-Temporal Patching*: We define a spatio-temporal patch $X_{k,t}$ of dimension $S_p \times T_p$, where S_p is the derived spatial cluster and T_p is the temporal window, effectively transforming irregular spatial structures into regular patch samples.

4.2.3 Discussion.

Why Greedy Clustering over Convolution Operator? Traditional convolution or graph operator require adjacency matrices N_A , complicating batch processing across heterogeneous cities (where $N_A \neq N_B$). In contrast, our approach renders tokens structurally independent, enabling massive parallel training for efficient scaling. Furthermore, by enforcing local aggregation via KD-Tree, we explicitly encode the geoscience principle that “near things are more related” into tokenization. The attention mechanism subsequently learns global correlations among these local samples, effectively modeling the hierarchy of urban dynamics. Detailed pseudocode and visualizations of the greedy capacity-constrained clustering algorithm are provided in Appendix B.

4.3 Architecture Scaling

4.3.1 Intuition

Existing spatio-temporal models (Wu et al., 2019; Ma et al., 2025), even including current foundation models (Li et al., 2025; Yuan et al., 2025; Zhong et al., 2025), rely heavily on the injection of handcrafted priors, such as auxiliary graph structures or node prompts. While these priors yield benefits on limited datasets, the strong inductive biases they introduce inevitably become bottlenecks for scaling. We posit that the crux of urban modeling lies in capturing dynamic correlations. Consequently, our objective is to construct an architecture with minimal inductive bias, relying exclusively on the attention mechanism to learn evolving dependencies from massive data, rather than hard-coding human heuristics.

4.3.2 Solution

As shown in Figure 3 right, we design UrbanFM by streamlining standard transformer (Vaswani et al., 2017) components, only optimizing them specifically for spatio-temporal samples.

- *Factorized Spatio-Temporal Attention*: To preserve fine-grained dynamic relationships at the point level without incurring the quadratic complexity of standard self-attention on flattened sequences, we factorize the computation into two orthogonal phases:
 - ▶ *Temporal Attention*: we first use the self-attention layer to model temporal dependencies within each spatial node.

- ▶ *Spatial Attention*: we then use the self-attention layer to model spatial dependencies between nodes at each time step.
- *Spatio-Temporal RoPE*: Addressing the inherent permutation invariance of attention, we use RoPE (Sun et al., 2024) to encode relative positions by rotating query and key vectors in the embedding space:
 - ▶ *T-RoPE*: Encodes relative temporal distances, enabling the model to generalize to varying historical context lengths.
 - ▶ *S-RoPE*: Encodes relative spatial order within linearized samples, preserving local proximity without adjacency matrix.
- *RevIN & Generative Modeling*: To mitigate the non-stationary statistics of urban flows, we apply instance normalization before and after the backbone. We adopt modern generative modeling objective where future time steps are masked with zero noise values, compelling the model to reconstruct future signals from noisy contexts, thereby unifying forecasting and imputation.

4.3.3 Discussion

Rationale for Minimalist Design. Transformers have demonstrated clear scaling laws (Kaplan et al., 2020), where increasing depth and data volume consistently reduces loss. Therefore, we eschew superfluous structural priors, relying solely on self-attention to capture dynamics. Furthermore, this simplified design allows our model to leverage modern hardware optimizations and architectural iterations (Sun et al., 2025), such as Flash Attention (Dao et al., 2022) and Linear Attention (Katharopoulos et al., 2020), facilitating massive scaling. Additionally, our pre-training objective aligns with modern generative prediction paradigms, enabling the model to flexibly support arbitrary-length forecasting, a significant advantage over the fixed-length constraints of traditional models.

Ethics, Fairness, and Limitations are discussed in Appendix E.

5 Experiments

In this section, we conduct extensive experiments to investigate the following research questions:

- **RQ1**: Can UrbanFM match or surpass existing models in zero-shot and few-shot evaluations across various urban spatio-temporal analysis tasks? (**Effectiveness & Generality**)
- **RQ2**: Can the pre-training phase of UrbanFM benefit from the scaling of datasets and model capability? (**Scaling Property**)
- **RQ3**: Can the inference phase of UrbanFM robustly tolerate additional noise and meet the requirements of efficient inference in practical scenarios? (**Robustness & Efficiency**)

5.1 Experimental Setup

Benchmark Datasets and Baseline Settings. We constructed the largest and most comprehensive urban spatio-temporal benchmark to date, EvalST, comprising up to 12 datasets, for downstream task evaluation. EvalST encompasses real-world data in diverse formats (sensor-based and grid-based), spanning various domains such as traffic flow, speed, occupancy, road networks, bicycles, taxis, and trajectories, across 4 countries and 7 cities, and a temporal range exceeding 10 years. To facilitate comprehensive evaluation, we selected 22 diverse baseline models, including specialized expert models and foundation models. For forecasting tasks, the expert models consist of spatio-temporal graph models specifically designed for sensor-based data (STAEformer (Liu et al., 2023), STID (Shao et al., 2022a), D2STGNN (Shao et al., 2022b), GWNET (Wu et al., 2019)) and spatio-temporal grid models tailored for grid-based data (TAU (Tan et al., 2023), PredRNN++ (Wang et al., 2022), DSAN (Lin et al., 2020), ST-ResNet (Zhang et al., 2017)). Notably, spatio-temporal grid models cannot be applied to sensor-based datasets, and adjacency matrices for spatio-temporal graph models were pre-constructed based on the first-order adjacency of grids for application to grid-based datasets. The foundation models include time series foundation models (TimesFM++ (Das et al., 2024), Moirai (Woo et al., 2024), Time-MoE (Shi et al., 2025), Chronos (Ansari et al., 2024)) and spatio-temporal foundation

models (FactoST (Zhong et al., 2026, 2025), OpenCity (Li et al., 2025)). Notably, for open-source foundation models, we evaluate their zero-shot performance using publicly available weights, reporting the optimal results. For closed-source counterparts, we retrain them following the original literature to ensure a fair and unified comparison. For imputation tasks, we choose classical method (Mean, *KNN* (Crookston and Finley, 2008), *MICE* (Van Buuren and Groothuis-Oudshoorn, 2011), and *SVDImpute* (Xu et al., 2017)) as default baselines. More details about the baselines and operations are provided in Appendix C.1 and C.2.

Evaluation Protocols and Settings. Spatio-temporal data in each dataset are chronologically partitioned into training, validation, and testing sets (6:2:2) with early stopping applied. We evaluate three configurations: *full-shot* (standard training), *few-shot* (training / fine-tuning on 10% of train set), and *zero-shot* (direct inference for foundation models). Following standard protocols (Shao et al., 2024; Cini et al., 2022), the look-back and horizon windows are set to 12 steps for *short-term* and 24 steps for *long-term forecasting*. For imputation tasks, we simulate *block missing* (5% sensor drop rate per step) and *point missing* (25% random masking). Performance is measured via MAE, RMSE, and MAPE. Regarding hyper-parameters, patch sizes S_p and T_p for MiniST tokenization are set to 16 and 48, while UrbanFM defaults to 8 layers (4 spatial, 4 temporal) with 10 pre-training epochs. Further evaluation and parameter details are provided in Appendix C.3.

5.2 Performance Evaluation (RQ1)

To evaluate the effectiveness of UrbanFM, we conducted a comprehensive comparison with 22 baselines, and we present the average MAPE across each dataset as a comprehensive indicator analysis.

5.2.1 Zero-Shot Generalization

Figure 5 illustrates the zero-shot performance of UrbanFM across both sensor-based and grid-based benchmarks for short-term and long-term forecasting. We observe several key findings: **① Significant Superiority over Existing Foundation Models:** UrbanFM consistently achieves the lowest MAPE across all scenarios. In both sensor- and grid-based zero-shot benchmarks, UrbanFM substantially outperforms existing spatio-temporal foundation models, with performance gains ranging from 39.0% to 70.2%. This suggests that the large-scale pre-training paradigm of UrbanFM effectively captures universal laws governing urban spatio-temporal patterns. **② Outperforming Domain-Specific Experts:** Notably, even in a zero-shot setting, UrbanFM’s performance is comparable to, or even surpasses, expert models trained on the full target dataset (full-shot). For instance, in long-term sensor-based forecasting, UrbanFM (17.0) outperforms highly specialized models such as D2STGNN (20.5) and STID (19.9). **③ Robustness Across Data Structures and Horizons:** UrbanFM maintains a decisive lead in both short- and long-term horizons across grid and sensor data. This demonstrates its architectural flexibility in handling heterogeneous urban data representations and its long-term predictive stability.

5.2.2 Adaptability and Few-Shot Performance

Figure 5 depicts the performance gains of UrbanFM when adapting to target domains via few-shot fine-tuning. We observe that: **① Substantial Performance Gains:** UrbanFM exhibits remarkable "rapid adaptation" capabilities. With fine-tuning on only a small fraction of target samples, UrbanFM’s performance further exceeds that of full-shot expert models, with relative improvements of 28.2%–65.2%. **② Efficient Adaptation:** Compared to other foundation models, UrbanFM achieves superior performance increments. Even while maintaining a lower baseline error, our model yields relative improvements of 19.1%–62.8% over competing foundation models. While other models show some gains, their final error rates remain significantly higher than UrbanFM’s few-shot results. **③ Adaptability to Sparse Data Domains:** The few-shot performance boost is particularly pronounced in grid-based tasks. We attribute this to the fact that while the pre-training set contained fewer grid-style datasets, our data scaling strategy allows the model to quickly align with the target distribution of sparse domains through minimal supervision.

5.2.3 Cross-Task Generalization

Figure 6 presents the performance of UrbanFM on spatio-temporal data imputation tasks across four PEMS benchmarks. We evaluate the model under two challenging scenarios: *point imputation* (random missing values)

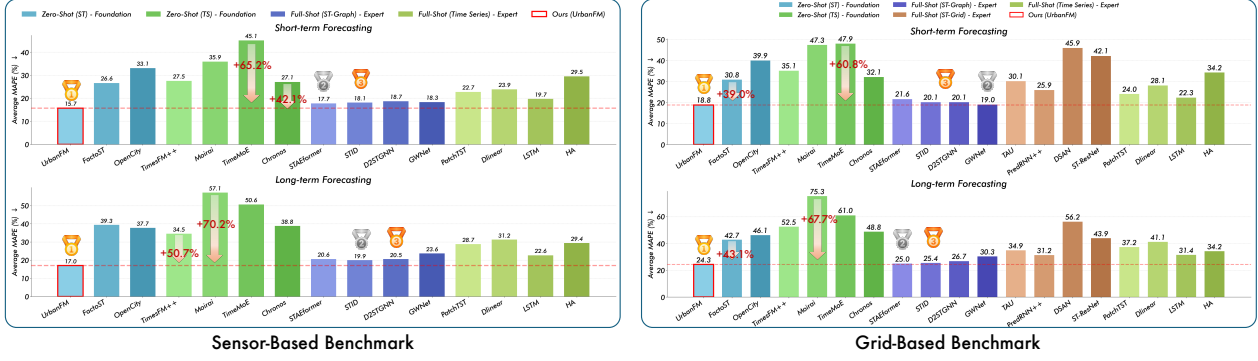


Figure 4 Zero-shot forecasting effectiveness on various spatial-temporal benchmarks (Full results in Table D.1, D.2, D.3, and D.4).

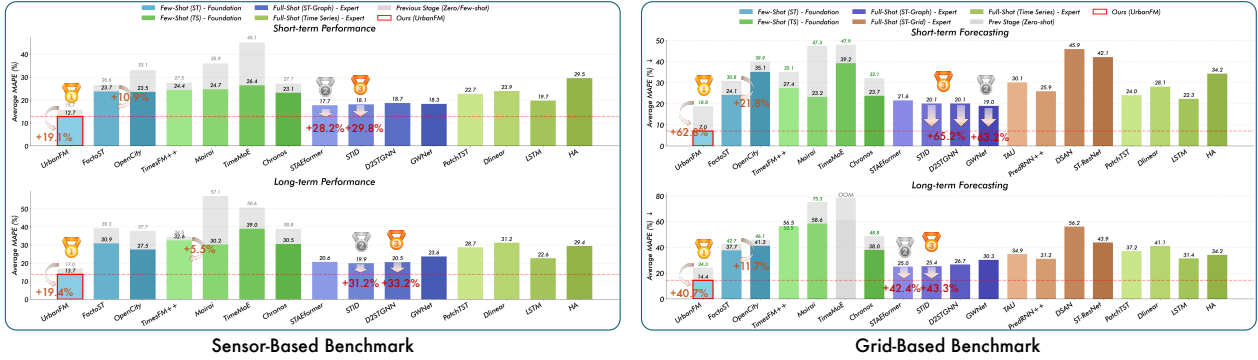


Figure 5 Evaluation of UrbanFM's performance gain through few-shot tuning and comparison with full-shot expert models.

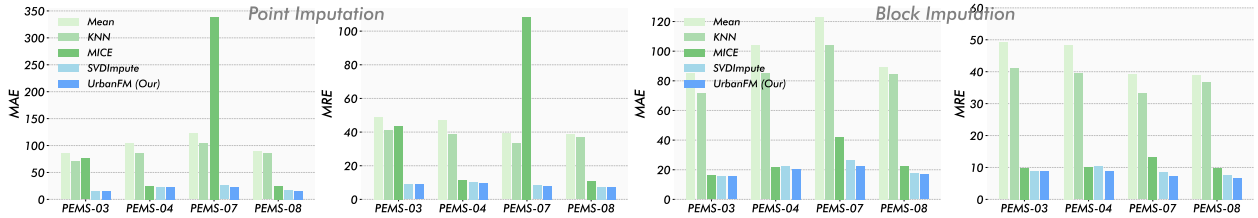


Figure 6 Performance evaluation of UrbanFM and classic methods for spatio-temporal point and block data imputation tasks.

and *block imputation* (continuous missing time intervals). **1** *Exceptional Zero-Shot Transferability*: Despite the absence of imputation learning objectives during the pre-training phase, **UrbanFM** consistently achieves the lowest error rates across all PEMS datasets. We attribute this success to our generative modeling strategy, which enables the model to leverage universal spatio-temporal representations learned from forecasting tasks effectively. **2** *Robustness to Complex Missing Patterns*: In the highly challenging *block imputation* scenario, **UrbanFM** leverages learned spatio-temporal structural priors to accurately reconstruct long-range missing segments. Consequently, it significantly outperforms traditional baselines such as MICE and SVD. **3** *High Stability Across Datasets*: In contrast to baselines like MICE, which exhibit high variance (e.g., instability on PEMS-07), our model maintains consistently low error bounds across diverse traffic distributions. This validates the robustness of **UrbanFM** as a reliable backbone for urban data analysis.

5.3 Scaling Evaluation (RQ2)

5.3.1 Scaling Property of Model Side

Model depth analysis (Figure 7, row 1) shows that on all PEMS datasets, increasing the number of Attention layers from 2 to 8 consistently reduces both short-term and long-term prediction errors. This performance

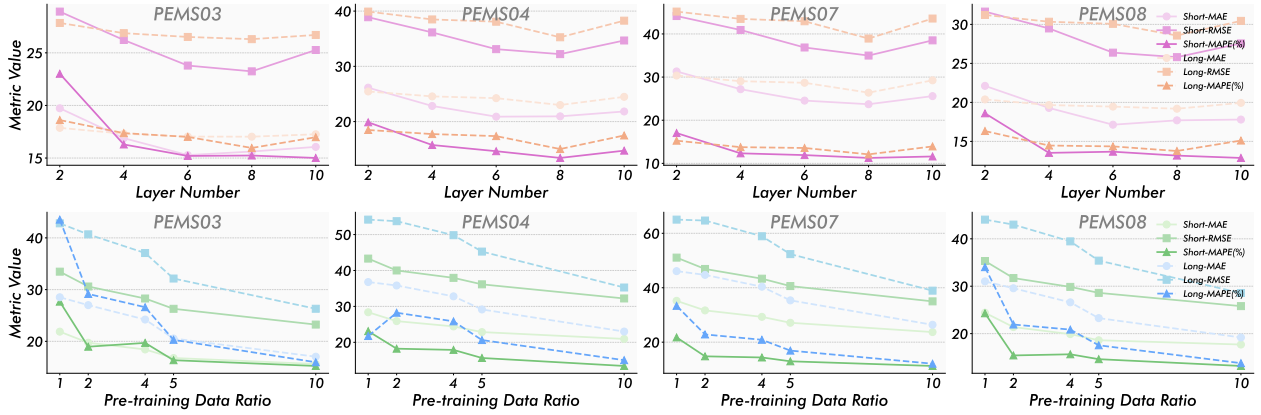


Figure 7 Scaling law analysis across model depth, data volume. (Full results in Table D.5 and D.6).

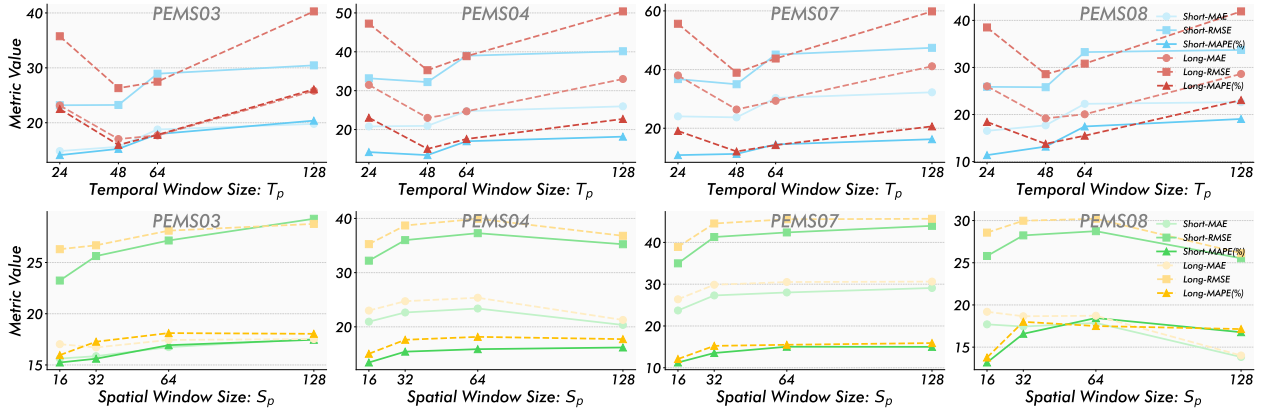


Figure 8 Scaling law analysis of spatio-temporal resolutions (Full results in Table D.7 and D.8).

improvement stems from the enhanced ability of deeper architectures to capture spatiotemporal hierarchical dependencies. For larger parameters, we consider this a future engineering optimization challenge.

5.3.2 Scaling Property of Data Side

The effect of expanding the pre-training data volume (Figure 7, row 2) shows that MAE, RMSE, and MAPE all exhibit power-law decay as the data proportion gradually increases from 1%. No performance saturation was observed at the maximum test proportion, confirming that **UrbanFM** can effectively extract generalized urban dynamic features from large-scale corpora. This indicates that further data expansion will continue to enhance its zero-shot generalization ability.

5.3.3 Scaling Property of Sample Side

The evaluation of the spatiotemporal window size (Figure 8) shows that model performance is highly sensitive to the range of the input context. Although increasing the temporal window (T_p) and spatial window (S_p) can initially improve accuracy by expanding the receptive field, performance usually tends to stabilize or slightly decrease after exceeding a certain threshold (*e.g.*, 64), reflecting the inherent locality of urban patterns, where excessive context introduces weak noise.

5.4 Deployment Evaluation (RQ3)

5.4.1 Robustness Study

To evaluate **UrbanFM**'s resilience against real-world sensor outages and transmission errors, we conducted a case study of stress tests using 30% zero-masking and 30% Gaussian noise injection. Observations from

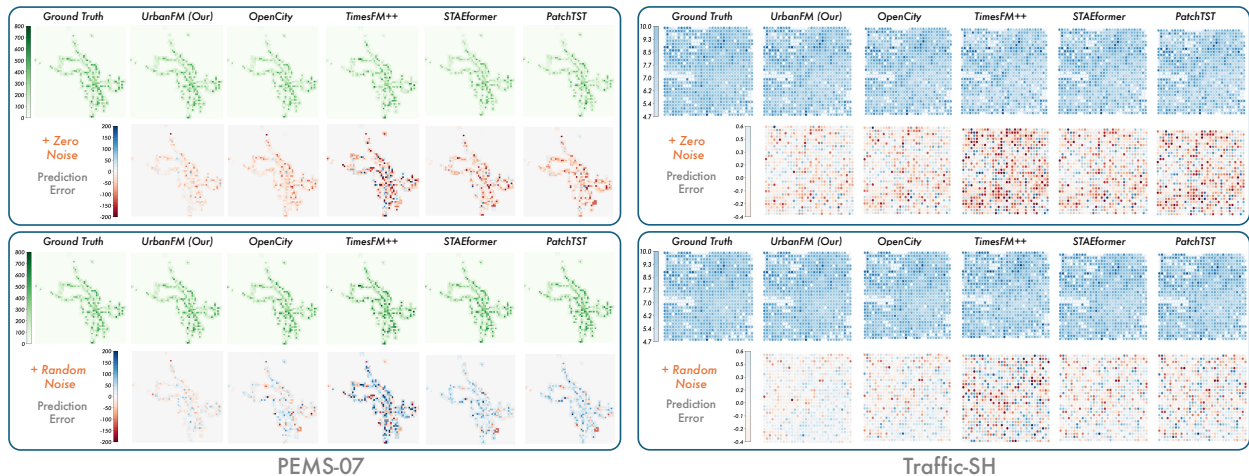


Figure 9 A visualization study of the robustness of predictions in noisy environments using two datasets.

Figure 9 reveal three key phenomena: ❶ *ST-FM Superiority*: Unlike specialized experts (e.g., STAEformer) that suffer significant degradation due to distribution shifts, our **UrbanFM** and **OpenCity** demonstrates superior robustness, avoiding the high-error regions typical of overfitted models. ❷ *Role of Spatial Coupling*: While time-series foundation models struggle with spatial consistency, **UrbanFM** leverages spatio-temporal correlations to rectify local anomalies, resulting in significantly smoother error surfaces. ❸ *Intrinsic Denoising of UrbanFM*: **UrbanFM** maintains the highest fidelity across all scenarios. This resilience is attributed to our generative modeling pre-training, which treats signal recovery as a core objective, effectively enabling the model to treat data corruption as a routine inference task.

5.4.2 Efficiency Study

We evaluated the total inference time and predictive performance (MAPE) of **UrbanFM** against other state-of-the-art time series and foundation models. To ensure a fair comparison, we report the total inference time required to process the test set on the same hardware environment (One A100 GPU, 64 batch size, PEMS-03 short). As illustrated in Figure ??, **UrbanFM** strikes a favorable balance between forecasting accuracy and computational efficiency. Specifically: ❶ Compared to lightweight time series models (e.g., PatchTST), although they achieve marginally lower latency, their simplified designs lead to inferior forecasting performance (higher MAPE). ❷ Compared to large-scale foundation models (e.g., Chronos, TimeMoE, TimesFM++), our approach achieves superior performance (the lowest MAPE of 15.2%) while requiring orders of magnitude less inference time (e.g., roughly 4× faster than Chronos and 10× faster than TimeMoE), demonstrating the practical efficiency of our architecture in real-world deployments.

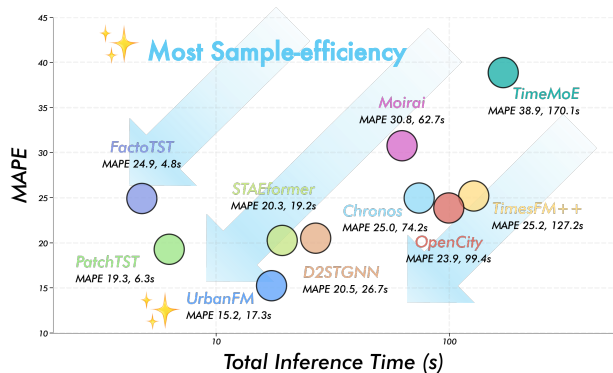


Figure 10 Efficiency study of our method.

6 Conclusion

In this work, we present a systematic investigation into urban spatio-temporal foundation models, aiming to transcend the fragmentation of existing scenario-specific approaches. Guided by the first principles of urban science (i.e., heterogeneity, correlation, and dynamics), we propose a unified scaling framework comprising **WorldST**, **MiniST**, **UrbanFM**, and **EvalST** to address *what* and *how* to scale. Extensive empirical results demonstrate that **UrbanFM** achieves remarkable zero-shot generalization capabilities previously unattainable by specialized baselines. We believe this work marks a pivotal paradigm shift, providing a blueprint for large-scale urban spatio-temporal intelligence research and advancing our understanding of complex city dynamics.

References

- Rui An, Yifeng Zhang, Ziran Liang, Wenqi Fan, Yuxuan Liang, Xuequn Shang, and Qing Li. Damba-st: Domain-adaptive mamba for efficient urban spatio-temporal prediction. 2026.
- Abdul Fatir Ansari, Lorenzo Stella, Ali Caner Turkmen, Xiyuan Zhang, Pedro Mercado, Huibin Shen, Oleksandr Shchur, Syama Sundar Rangapuram, Sebastian Pineda Arango, Shubham Kapoor, et al. Chronos: Learning the language of time series. Transactions on Machine Learning Research, 2024.
- Bahar Biller and Barry L Nelson. Modeling and generating multivariate time-series input processes using a vector autoregressive technique. ACM Transactions on Modeling and Computer Simulation (TOMACS), 13(3):211–237, 2003.
- George EP Box and David A Pierce. Distribution of residual autocorrelations in autoregressive-integrated moving average time series models. Journal of the American statistical Association, 65(332):1509–1526, 1970.
- Tom Brown, Benjamin Mann, Nick Ryder, Melanie Subbiah, Jared D Kaplan, Prafulla Dhariwal, Arvind Neelakantan, Pranav Shyam, Girish Sastry, Amanda Askell, et al. Language models are few-shot learners. Advances in neural information processing systems, 33:1877–1901, 2020.
- Hao Chen, Bhiksha Raj, Xing Xie, and Jindong Wang. On catastrophic inheritance of large foundation models. Journal of Data-centric Machine Learning Research, 2024a.
- Wei Chen and Yuxuan Liang. Expand and compress: Exploring tuning principles for continual spatio-temporal graph forecasting. In The Thirteenth International Conference on Learning Representations, 2025a.
- Wei Chen and Yuxuan Liang. Learning with calibration: Exploring test-time computing of spatio-temporal forecasting. In The Thirty-ninth Annual Conference on Neural Information Processing Systems, 2025b.
- Wei Chen, Yuxuan Liang, Yuanshao Zhu, Yanchuan Chang, Kang Luo, Haomin Wen, Lei Li, Yanwei Yu, Qingsong Wen, Chao Chen, et al. Deep learning for trajectory data management and mining: A survey and beyond. arXiv preprint arXiv:2403.14151, 2024b.
- Wei Chen, Yuqian Wu, Yuanshao Zhu, Xixuan Hao, Shiyu Wang, Xiaofang Zhou, and Yuxuan Liang. Select, then balance: A plug-and-play framework for exogenous-aware spatio-temporal forecasting. arXiv preprint arXiv:2509.05779, 2025.
- Andrea Cini, Ivan Marisca, and Cesare Alippi. Filling the g_ap_s: Multivariate time series imputation by graph neural networks. In International Conference on Learning Representations, 2022.
- Noel Cressie and Christopher K Wikle. Statistics for spatio-temporal data. John Wiley & Sons, 2011.
- Nicholas L Crookston and Andrew O Finley. yaimpute: an r package for knn imputation. Journal of Statistical Software, 23:1–16, 2008.
- Yue Cui, Jiandong Xie, and Kai Zheng. Historical inertia: A neglected but powerful baseline for long sequence time-series forecasting. In Proceedings of the 30th ACM international conference on information & knowledge management, pages 2965–2969, 2021.
- Tri Dao, Dan Fu, Stefano Ermon, Atri Rudra, and Christopher Ré. Flashattention: Fast and memory-efficient exact attention with io-awareness. Advances in neural information processing systems, 35:16344–16359, 2022.
- Abhimanyu Das, Weihao Kong, Rajat Sen, and Yichen Zhou. A decoder-only foundation model for time-series forecasting. In Ruslan Salakhutdinov, Zico Kolter, Katherine Heller, Adrian Weller, Nuria Oliver, Jonathan Scarlett, and Felix Berkenkamp, editors, Proceedings of the 41st International Conference on Machine Learning, volume 235 of Proceedings of Machine Learning Research, pages 10148–10167. PMLR, 21–27 Jul 2024.
- Michael Dietze, Ethan P White, Antoinette Abeyta, Carl Boettiger, Nievita Bueno Watts, Cayelan C Carey, Rebecca Chaplin-Kramer, Ryan E Emanuel, SK Morgan Ernest, Renato J Figueiredo, et al. Near-term ecological forecasting for climate change action. Nature Climate Change, 14(12):1236–1244, 2024.
- Lei Dong, Fabio Duarte, Gilles Duranton, Paolo Santi, Marc Barthelemy, Michael Batty, Luís Bettencourt, Michael Goodchild, Gary Hack, Yu Liu, et al. Defining a city—delineating urban areas using cell-phone data. Nature Cities, 1(2):117–125, 2024.
- Alireza Ermagun and David Levinson. Spatiotemporal traffic forecasting: review and proposed directions. Transport Reviews, 38(6):786–814, 2018.

- Yuchen Fang, Hao Miao, Yuxuan Liang, Liwei Deng, Yue Cui, Ximu Zeng, Yuyang Xia, Yan Zhao, Torben Bach Pedersen, Christian S Jensen, et al. Unraveling spatio-temporal foundation models via the pipeline lens: A comprehensive review. IEEE Transactions on Knowledge and Data Engineering, 2026.
- Haotian Gao, Renhe Jiang, Zheng Dong, Jinliang Deng, Yuxin Ma, and Xuan Song. Spatial-temporal-decoupled masked pre-training for spatiotemporal forecasting. In IJCAI, 2024.
- Nan Gao, Hao Xue, Wei Shao, Sichen Zhao, Kyle Kai Qin, Arian Prabowo, Mohammad Saiedur Rahaman, and Flora D Salim. Generative adversarial networks for spatio-temporal data: A survey. ACM Transactions on Intelligent Systems and Technology (TIST), 13(2):1–25, 2022.
- Shengnan Guo, Youfang Lin, Ning Feng, Chao Song, and Huaiyu Wan. Attention based spatial-temporal graph convolutional networks for traffic flow forecasting. In Proceedings of the AAAI conference on artificial intelligence, volume 33, pages 922–929, 2019.
- Oliver Hamelijnck, William Wilkinson, Niki Loppi, Arno Solin, and Theodoros Damoulas. Spatio-temporal variational gaussian processes. Advances in Neural Information Processing Systems, 34:23621–23633, 2021.
- Jindong Han, Weijia Zhang, Hao Liu, Tao Tao, Naiqiang Tan, and Hui Xiong. Bigst: Linear complexity spatio-temporal graph neural network for traffic forecasting on large-scale road networks. Proceedings of the VLDB Endowment, 17(5):1081–1090, 2024.
- Jindong Han, Hao Wang, Hui Xiong, and Hao Liu. Scalable pre-training of compact urban spatio-temporal predictive models on large-scale multi-domain data. Proceedings of the VLDB Endowment, 18(7):2149–2158, 2025.
- Sepp Hochreiter and Jürgen Schmidhuber. Long short-term memory. Neural computation, 9(8):1735–1780, 1997.
- Aaron Hurst, Adam Lerer, Adam P Goucher, Adam Perelman, Aditya Ramesh, Aidan Clark, AJ Ostrow, Akila Welihinda, Alan Hayes, Alec Radford, et al. Gpt-4o system card. arXiv preprint arXiv:2410.21276, 2024.
- Guangyin Jin, Yuxuan Liang, Yuchen Fang, Zezhi Shao, Jincai Huang, Junbo Zhang, and Yu Zheng. Spatio-temporal graph neural networks for predictive learning in urban computing: A survey. IEEE Transactions on Knowledge and Data Engineering, 36(10):5388–5408, 2023.
- Ming Jin, Huan Yee Koh, Qingsong Wen, Daniele Zambon, Cesare Alippi, Geoffrey I Webb, Irwin King, and Shirui Pan. A survey on graph neural networks for time series: Forecasting, classification, imputation, and anomaly detection. IEEE Transactions on Pattern Analysis and Machine Intelligence, 2024.
- Jared Kaplan, Sam McCandlish, Tom Henighan, Tom B Brown, Benjamin Chess, Rewon Child, Scott Gray, Alec Radford, Jeffrey Wu, and Dario Amodei. Scaling laws for neural language models. arXiv preprint arXiv:2001.08361, 2020.
- Angelos Katharopoulos, Apoorv Vyas, Nikolaos Pappas, and François Fleuret. Transformers are rnns: Fast autoregressive transformers with linear attention. In International conference on machine learning, pages 5156–5165. PMLR, 2020.
- Yaguang Li, Rose Yu, Cyrus Shahabi, and Yan Liu. Diffusion convolutional recurrent neural network: Data-driven traffic forecasting. In International Conference on Learning Representations, 2018.
- Zhonghang Li, Long Xia, Lei Shi, Yong Xu, Dawei Yin, and Chao Huang. Open spatio-temporal foundation models for traffic prediction. ACM Trans. Intell. Syst. Technol., 2025.
- Yuxuan Liang, Haomin Wen, Yutong Xia, Ming Jin, Bin Yang, Flora Salim, Qingsong Wen, Shirui Pan, and Gao Cong. Foundation models for spatio-temporal data science: A tutorial and survey. In Proceedings of the 31st ACM SIGKDD Conference on Knowledge Discovery and Data Mining V. 2, pages 6063–6073, 2025.
- Gengyu Lin, Zhengyang Zhou, Qihe Huang, Kuo Yang, Shifen Cheng, and Yang Wang. Fairstg: Countering performance heterogeneity via collaborative sample-level optimization. IEEE Transactions on Mobile Computing, 2024.
- Haoxing Lin, Rufan Bai, Weijia Jia, Xinyu Yang, and Yongjian You. Preserving dynamic attention for long-term spatial-temporal prediction. In Proceedings of the 26th ACM SIGKDD International Conference on Knowledge Discovery & Data Mining, pages 36–46, 2020.
- Aoyu Liu and Yaying Zhang. Crossst: An efficient pre-training framework for cross-district pattern generalization in urban spatio-temporal forecasting. In 2025 IEEE 41st International Conference on Data Engineering (ICDE), pages 2935–2948. IEEE, 2025.

- Chenxi Liu, Kethmi Hirushini Hettige, Qianxiong Xu, Cheng Long, Shili Xiang, Gao Cong, Ziyue Li, and Rui Zhao. St-llm+: Graph enhanced spatio-temporal large language models for traffic prediction. IEEE Transactions on Knowledge and Data Engineering, 2025a.
- Hangchen Liu, Zheng Dong, Renhe Jiang, Jiewen Deng, Jinliang Deng, Qianjun Chen, and Xuan Song. Spatio-temporal adaptive embedding makes vanilla transformer sota for traffic forecasting. In Proceedings of the 32nd ACM international conference on information and knowledge management, pages 4125–4129, 2023.
- Lingbo Liu, Jiajie Zhen, Guanbin Li, Geng Zhan, Zhaocheng He, Bowen Du, and Liang Lin. Dynamic spatial-temporal representation learning for traffic flow prediction. IEEE Transactions on Intelligent Transportation Systems, 22(11): 7169–7183, 2020.
- Yuhang Liu, Yingxue Zhang, Xin Zhang, Ling Tian, Yanhua Li, and Jun Luo. Urbanmind: Urban dynamics prediction with multifaceted spatial-temporal large language models. In Proceedings of the 31st ACM SIGKDD Conference on Knowledge Discovery and Data Mining V. 2, pages 1951–1962, 2025b.
- Jiaming Ma, Binwu Wang, Guanjun Wang, Kuo Yang, Zhengyang Zhou, Pengkun Wang, Xu Wang, and Yang Wang. Less but more: Linear adaptive graph learning empowering spatiotemporal forecasting. In The Thirty-ninth Annual Conference on Neural Information Processing Systems, 2025.
- Ivan Marisca, Cesare Alippi, and Filippo Maria Bianchi. Graph-based forecasting with missing data through spatiotemporal downsampling. In International Conference on Machine Learning, pages 34846–34865. PMLR, 2024.
- Tong Nie, Guoyang Qin, Wei Ma, Yuewen Mei, and Jian Sun. Imputeformer: Low rankness-induced transformers for generalizable spatiotemporal imputation. In Proceedings of the 30th ACM SIGKDD Conference on Knowledge Discovery and Data Mining, pages 2260–2271, 2024.
- Y Nie. A time series is worth 64words: Long-term forecasting with transformers. arXiv preprint arXiv:2211.14730, 2022.
- Luca Pappalardo, Ed Manley, Vedran Sekara, and Laura Alessandretti. Future directions in human mobility science. Nature computational science, 3(7):588–600, 2023.
- H. Qu, Y. Gong, M. Chen, J. Zhang, Y. Zheng, and Y. Yin. Forecasting fine-grained urban flows via spatio-temporal contrastive self-supervision. IEEE Transactions on Knowledge & Data Engineering, 2022.
- Hanan Samet. Foundations of multidimensional and metric data structures. Morgan Kaufmann, 2006.
- ZeZhi Shao, Zhao Zhang, Fei Wang, Wei Wei, and Yongjun Xu. Spatial-temporal identity: A simple yet effective baseline for multivariate time series forecasting. In Proceedings of the 31st ACM International Conference on Information & Knowledge Management, pages 4454–4458, 2022a.
- ZeZhi Shao, Zhao Zhang, Wei Wei, Fei Wang, Yongjun Xu, Xin Cao, and Christian S Jensen. Decoupled dynamic spatial-temporal graph neural network for traffic forecasting. Proceedings of the VLDB Endowment, 15(11):2733–2746, 2022b.
- ZeZhi Shao, Fei Wang, Yongjun Xu, Wei Wei, Chengqing Yu, Zhao Zhang, Di Yao, Tao Sun, Guangyin Jin, Xin Cao, et al. Exploring progress in multivariate time series forecasting: Comprehensive benchmarking and heterogeneity analysis. IEEE Transactions on Knowledge and Data Engineering, 2024.
- Xiaoming Shi, Shiyu Wang, Yuqi Nie, Dianqi Li, Zhou Ye, Qingsong Wen, and Ming Jin. Time-moe: Billion-scale time series foundation models with mixture of experts. In The Thirteenth International Conference on Learning Representations, 2025.
- Xingjian Shi and Dit-Yan Yeung. Machine learning for spatiotemporal sequence forecasting: A survey. arXiv preprint arXiv:1808.06865, 2018.
- Chao Song, Youfang Lin, Shengnan Guo, and Huaiyu Wan. Spatial-temporal synchronous graph convolutional networks: A new framework for spatial-temporal network data forecasting. In Proceedings of the AAAI conference on artificial intelligence, volume 34, pages 914–921, 2020.
- Jianlin Su, Murtadha Ahmed, Yu Lu, Shengfeng Pan, Wen Bo, and Yunfeng Liu. Roformer: Enhanced transformer with rotary position embedding. Neurocomputing, 568:127063, 2024.
- Weigao Sun, Jiayi Hu, Yucheng Zhou, Jusen Du, Disen Lan, Kexin Wang, Tong Zhu, Xiaoye Qu, Yu Zhang, Xiaoyu Mo, et al. Speed always wins: A survey on efficient architectures for large language models. arXiv preprint arXiv:2508.09834, 2025.

- Richard Sutton. The bitter lesson. Incomplete Ideas (blog), 13(1):38, 2019.
- Cheng Tan, Zhangyang Gao, Lirong Wu, Yongjie Xu, Jun Xia, Siyuan Li, and Stan Z Li. Temporal attention unit: Towards efficient spatiotemporal predictive learning. In Proceedings of the IEEE/CVF conference on computer vision and pattern recognition, pages 18770–18782, 2023.
- Chen Tang, Xinzhu Ma, Encheng Su, Xiufeng Song, Xiaohong Liu, Wei-Hong Li, Lei Bai, Wanli Ouyang, and Xiangyu Yue. Unistd: Towards unified spatio-temporal learning across diverse disciplines. In Proceedings of the Computer Vision and Pattern Recognition Conference, pages 29213–29224, 2025.
- Stefan Thurner, Rudolf Hanel, and Peter Klimek. Introduction to the theory of complex systems. Oxford University Press, 2018.
- Waldo R Tobler. A computer movie simulating urban growth in the detroit region. Economic geography, 46(sup1): 234–240, 1970.
- Stef Van Buuren and Karin Groothuis-Oudshoorn. mice: Multivariate imputation by chained equations in r. Journal of statistical software, 45:1–67, 2011.
- Ashish Vaswani, Noam Shazeer, Niki Parmar, Jakob Uszkoreit, Llion Jones, Aidan N Gomez, Łukasz Kaiser, and Illia Polosukhin. Attention is all you need. Advances in neural information processing systems, 30, 2017.
- Senzhang Wang, Jiannong Cao, and S Yu Philip. Deep learning for spatio-temporal data mining: A survey. IEEE transactions on knowledge and data engineering, 34(8):3681–3700, 2020.
- Yunbo Wang, Haixu Wu, Jianjin Zhang, Zhifeng Gao, Jianmin Wang, S Yu Philip, and Mingsheng Long. Predrnn: A recurrent neural network for spatiotemporal predictive learning. IEEE Transactions on Pattern Analysis and Machine Intelligence, 45(2):2208–2225, 2022.
- Gerald Woo, Chenghao Liu, Akshat Kumar, Caiming Xiong, Silvio Savarese, and Doyen Sahoo. Unified training of universal time series forecasting transformers. In Ruslan Salakhutdinov, Zico Kolter, Katherine Heller, Adrian Weller, Nuria Oliver, Jonathan Scarlett, and Felix Berkenkamp, editors, Proceedings of the 41st International Conference on Machine Learning, volume 235 of Proceedings of Machine Learning Research, pages 53140–53164. PMLR, 21–27 Jul 2024.
- Hao Wu, Yuan Gao, Xingjian Shi, Shuai Peng Li, Fan Xu, Fan Zhang, Zhihong Zhu, Weiyan Wang, Xiao Luo, Kun Wang, et al. Spatiotemporal forecasting as planning: A model-based reinforcement learning approach with generative world models. arXiv preprint arXiv:2510.04020, 2025a.
- Yuqian Wu, Yuhong Peng, Jiapeng Yu, and Raymond Lee. Mas4poi: a multi-agents collaboration system for next poi recommendation. In Pacific-Asia Conference on Knowledge Discovery and Data Mining, pages 356–367. Springer, 2025b.
- Yuqian Wu, Yuhong Peng, Jiapeng Yu, Xiangyu Liu, Zeting Yan, Kang Lin, Weifeng Su, Bingqing Qu, Raymond Lee, and Dingqi Yang. Beyond regularity: Modeling chaotic mobility patterns for next location prediction. arXiv preprint arXiv:2509.11713, 2025c.
- Zonghan Wu, Shirui Pan, Guodong Long, Jing Jiang, and Chengqi Zhang. Graph wavenet for deep spatial-temporal graph modeling. In Proceedings of the 28th International Joint Conference on Artificial Intelligence, pages 1907–1913, 2019.
- Peipei Xu, Wenjie Ruan, Quan Z Sheng, Tao Gu, and Lina Yao. Interpolating the missing values for multi-dimensional spatial-temporal sensor data: a tensor svd approach. In Proceedings of the 14th EAI international conference on mobile and ubiquitous systems: computing, networking and services, pages 442–451, 2017.
- Xie Yu, Jingyuan Wang, Yifan Yang, Qian Huang, and Ke Qu. Bigcity: A universal spatiotemporal model for unified trajectory and traffic state data analysis. In 2025 IEEE 41st International Conference on Data Engineering (ICDE), pages 4455–4469. IEEE, 2025.
- Yuan Yuan, Jingtao Ding, Jie Feng, Depeng Jin, and Yong Li. Unist: A prompt-empowered universal model for urban spatio-temporal prediction. In Proceedings of the 30th ACM SIGKDD Conference on Knowledge Discovery and Data Mining, pages 4095–4106, 2024a.
- Yuan Yuan, Jingtao Ding, Chonghua Han, Zhi Sheng, Depeng Jin, and Yong Li. Uniflow: A foundation model for unified urban spatio-temporal flow prediction. arXiv preprint arXiv:2411.12972, 2024b.

- Yuan Yuan, Chonghua Han, Jingtao Ding, Guozhen Zhang, Depeng Jin, and Yong Li. Diffusion transformers as open-world spatiotemporal foundation models. In The Thirty-ninth Annual Conference on Neural Information Processing Systems, 2025.
- Ailing Zeng, Muxi Chen, Lei Zhang, and Qiang Xu. Are transformers effective for time series forecasting? In Proceedings of the AAAI conference on artificial intelligence, volume 37, pages 11121–11128, 2023.
- Junbo Zhang, Yu Zheng, and Dekang Qi. Deep spatio-temporal residual networks for citywide crowd flows prediction. In Proceedings of the AAAI conference on artificial intelligence, volume 31, 2017.
- Weijia Zhang, Jindong Han, Zhao Xu, Hang Ni, Hao Liu, and Hui Xiong. Urban foundation models: A survey. In Proceedings of the 30th ACM SIGKDD Conference on Knowledge Discovery and Data Mining, pages 6633–6643, 2024.
- Xiao Zheng, Saeed Asadi Bagloee, and Majid Sarvi. Treck: Long-term traffic forecasting with contrastive representation learning. IEEE Transactions on Intelligent Transportation Systems, 2024.
- Siru Zhong, Junjie Qiu, Yangyu Wu, Xingchen Zou, Zhongwen Rao, Bin Yang, Chenjuan Guo, Hao Xu, and Yuxuan Liang. Learning to factorize spatio-temporal foundation models. In The Thirty-ninth Annual Conference on Neural Information Processing Systems, 2025.
- Siru Zhong, Junjie Qiu, Yangyu Wu, Yiqiu Liu, Yuanpeng He, Zhongwen Rao, Bin Yang, Chenjuan Guo, Hao Xu, and Yuxuan Liang. Learning to factorize and adapt: A versatile approach toward universal spatio-temporal foundation models. arXiv preprint arXiv:2601.12083, 2026.

Appendix

Table of Contents

A Datasets Details	19
A.1 Evaluation Benchmark: EvalST	19
A.2 Pre-training Dataset: WorldST	20
B Method Detail	22
C Experimental Details	25
C.1 Baseline Details	25
C.1.1 Time Series Models	25
C.1.2 ST-Grid Models	25
C.1.3 ST-Graph Models	25
C.1.4 Time Series Foundation Models	26
C.1.5 Spatio-Temporal Foundation Models	26
C.1.6 Imputation Models	26
C.2 Details of Predefined Graph Construction	27
C.2.1 Distance-based Graph.	27
C.2.2 Grid-based Graph.	27
C.3 Protocol Details	27
C.3.1 Metrics Detail.	27
C.3.2 Parameter Detail.	27
D More Experimental Results	28
D.1 More Result on Performance Evaluation	28
D.2 More Result on Scaling Evaluation	28
E More Discussion	28
E.1 Ethics, Fairness, and Limitations	28
E.1.1 Privacy and Anonymity.	32
E.1.2 Fairness in Modeling.	32
E.1.3 Limitations.	32
E.2 Future Direction	32
E.2.1 Democratizing Urban AI via Few-Shot Transfer.	32
E.2.2 Multi-Modal Alignment with LLMs.	33
E.2.3 From Forecasting to Decision Making.	33

A Datasets Details

A.1 Evaluation Benchmark: EvalST

We first provide the statistical information of the evaluation benchmark as shown in Table A.1. Then, we visualize its spatial, temporal, and overall spatio-temporal distribution as shown in Figures A.1, A.2, and A.3.

Table A.1 Evaluation Benchmark Summary

Data Format	Domain Type	Dataset Name	Spatial Region	# Spatial Location	Temporal Range	# Temporal Step	Overlap
Sensor-based	Flow	PEMS-03	Los Angles, US	358	2018/09/01 – 2018/11/30	26208	×
		PEMS-04	Los Angles, US	307	2018/01/01 – 2018/02/28	16992	×
		PEMS-07	Los Angles, US	883	2017/05/01 – 2017/08/06	28224	×
		PEMS-08	Los Angles, US	170	2016/07/01 – 2016/08/31	17856	×
	Occupancy	OCC-Pairs	Pairs, FR	106	2016/01/01 – 2016/12/01	96410	×
		OCC-Hamburg	Hamburg, DE	240	2016/08/27 – 2016/12/09	30085	×
	Speed	PEMS-BAY	Los Angles, US	325	2017/01/01 – 2017/06/30	52116	×
		METR-LA	Los Angles, US	207	2012/03/01 – 2012/06/27	34272	×
Grid-based	Road	Traffic-SH	Shanghai, CN	$28 \times 32 = 896$	2022/01/27 – 2022/02/25	8413	×
	Bike	Bike-NYC	New York, US	$20 \times 10 = 200$	2016/07/01 – 2016/08/29	17275	×
	Taxi	Taxi-NYC	New York, US	$20 \times 10 = 200$	2015/01/01 – 2015/03/31	17275	×
	Trajectory	Tdrive-BJ	Beijing, CN	$28 \times 32 = 896$	2015/03/01 – 2015/06/30	35125	×

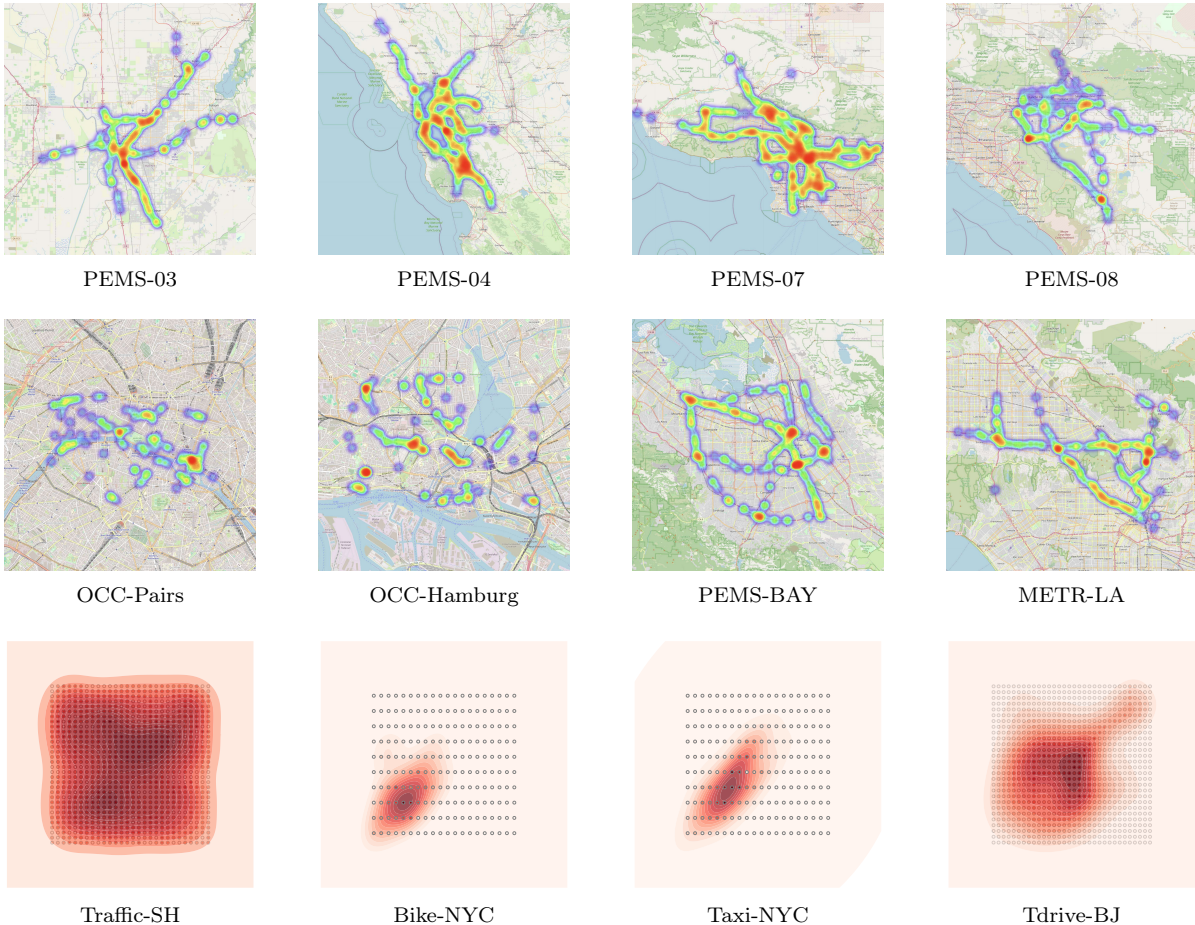


Figure A.1 Spatial Visualization of EvalSTBenchmark.

A.2 Pre-training Dataset: WorldST

We then provide statistics on the collected dataset WorldST that can be used for pre-training, as shown in Table A.2.

Table A.2 Pre-training Datasets Summary

Data Format	Domain Type	Spatial Region	# Spatial Location	Temporal Range	# Temporal Step
Sensor	Flow	Augsburg, DE	40	2017/05/06 – 2017/05/25	5757
Sensor	Flow	Basel, CH	66	2016/10/24 – 2016/10/31	2016
Sensor	Flow	Bern, CH	708	2016/10/24 – 2016/10/31	2016
Sensor	Flow	Birmingham, GB	34	2017/10/23 – 2017/11/18	7540
Sensor	Flow	Bolton, GB	56	2017/11/13 – 2017/11/18	1491
Sensor	Flow	Bordeaux, FR	409	2016/11/21 – 2016/11/27	2016
Sensor	Flow	Bremen, DE	518	2016/09/19 – 2016/10/02	4032
Sensor	Flow	Cagliari, IT	85	2016/05/16 – 2016/07/29	21600
Sensor	Flow	Constance, DE	113	2017/02/13 – 2017/02/19	2015
Sensor	Flow	Darmstadt, DE	163	2015/09/21 – 2016/05/06	65952
Sensor	Flow	Essen, DE	36	2017/03/27 – 2017/09/30	54023
Sensor	Flow	Frankfurt, DE	73	2016/12/21 – 2016/12/21	288
Sensor	Flow	Graz, AT	272	2016/04/04 – 2016/09/23	49823
Sensor	Flow	Groningen, NL	52	2017/09/21 – 2017/10/06	4584
Sensor	Flow	Hamburg, DE	376	2016/08/27 – 2016/12/09	30085
Sensor	Flow	Innsbruck, AT	16	2017/04/01 – 2017/04/30	8639
Sensor	Flow	Kassel, DE	234	2016/08/28 – 2016/09/02	1177
Sensor	Flow	London, GB	4130	2015/05/15 – 2016/05/22	107712
Sensor	Flow	Los Angeles, US	957	2017/10/02 – 2017/10/10	2592
Sensor	Flow	Luzern, CH	134	2015/01/01 – 2016/01/01	105121
Sensor	Flow	Madrid, ES	1065	2016/08/29 – 2017/11/11	126549
Sensor	Flow	Manchester, GB	114	2017/09/08 – 2017/11/18	20497
Sensor	Flow	Marseille, FR	164	2017/06/01 – 2017/07/01	8641
Sensor	Flow	Melbourne, AU	861	2018/02/12 – 2018/02/26	4318
Sensor	Flow	Munich, DE	509	2017/02/14 – 2017/02/15	288
Sensor	Flow	Paris, FR	169	2016/01/01 – 2016/12/01	96469
Sensor	Flow	Rotterdam, NL	230	2017/09/21 – 2017/11/02	12276
Sensor	Flow	Santander, ES	211	2016/06/17 – 2016/12/02	48359
Sensor	Flow	Stuttgart, DE	177	2016/03/21 – 2016/07/22	35711
Sensor	Flow	Taipei, CN-TW	275	2017/09/18 – 2017/10/01	4032
Sensor	Flow	Torino, IT	267	2016/09/26 – 2016/10/16	6048
Sensor	Flow	Toronto, CA	151	2016/09/01 – 2017/01/31	44062
Sensor	Flow	Toulouse, FR	469	2008/05/16 – 2008/06/27	12384
Sensor	Flow	Utrecht, NL	865	2017/06/12 – 2017/06/15	1152
Sensor	Flow	Vilnius, LT	9	2015/03/17 – 2015/03/18	289
Sensor	Flow	Wolfsburg, DE	103	2016/09/19 – 2016/10/02	4032
Sensor	Flow	Zurich, CH	996	2015/10/26 – 2015/11/01	2016
Sensor	Flow	Sydney, AU	27	2013/01/02 – 2024/05/31	4169

Table A.2 Pre-training Datasets Summary

Data Format	Domain Type	Spatial Region	# Spatial Location	Temporal Range	# Temporal Step
Sensor	Occupancy	Augsburg, DE	35	2017/05/06 – 2017/05/25	5757
Sensor	Occupancy	Basel, CH	47	2016/10/24 – 2016/10/31	2016
Sensor	Occupancy	Bern, CH	496	2016/10/24 – 2016/10/31	2016
Sensor	Occupancy	Bolton, GB	49	2017/11/13 – 2017/11/18	1491
Sensor	Occupancy	Bordeaux, FR	198	2016/11/21 – 2016/11/27	2016
Sensor	Occupancy	Bremen, DE	365	2016/09/19 – 2016/10/02	4032
Sensor	Occupancy	Cagliari, IT	61	2016/05/16 – 2016/07/29	21600
Sensor	Occupancy	Constance, DE	103	2017/02/13 – 2017/02/19	2015
Sensor	Occupancy	Darmstadt, DE	101	2015/09/21 – 2016/05/06	65952
Sensor	Occupancy	Essen, DE	24	2017/03/27 – 2017/09/30	54023
Sensor	Occupancy	Frankfurt, DE	59	2016/12/21 – 2016/12/21	288
Sensor	Occupancy	Graz, AT	232	2016/04/04 – 2016/09/23	49823
Sensor	Occupancy	Groningen, NL	42	2017/09/21 – 2017/10/06	4584
Sensor	Occupancy	Kassel, DE	179	2016/08/28 – 2016/09/02	1177
Sensor	Occupancy	London, GB	2793	2015/05/15 – 2016/05/22	107712
Sensor	Occupancy	Luzern, CH	108	2015/01/01 – 2016/01/01	105121
Sensor	Occupancy	Madrid, ES	659	2016/08/29 – 2017/11/11	126549
Sensor	Occupancy	Manchester, GB	15	2017/09/08 – 2017/11/18	20497
Sensor	Occupancy	Marseille, FR	115	2017/06/01 – 2017/07/01	8641
Sensor	Occupancy	Munich, DE	322	2017/02/14 – 2017/02/15	288
Sensor	Occupancy	Rotterdam, NL	108	2017/09/21 – 2017/11/02	12276
Sensor	Occupancy	Santander, ES	157	2016/06/17 – 2016/12/02	48359
Sensor	Occupancy	Speyer, DE	118	2016/09/19 – 2016/10/02	4032
Sensor	Occupancy	Strasbourg, FR	82	2017/05/10 – 2017/11/11	53221
Sensor	Occupancy	Stuttgart, DE	137	2016/03/21 – 2016/07/22	35711
Sensor	Occupancy	Taipei, CN-TW	227	2017/09/18 – 2017/10/01	4032
Sensor	Occupancy	Torino, IT	228	2016/09/26 – 2016/10/16	6048
Sensor	Occupancy	Toulouse, FR	364	2008/05/16 – 2008/06/27	12384
Sensor	Occupancy	Vilnius, LT	8	2015/03/17 – 2015/03/18	289
Sensor	Occupancy	Wolfsburg, DE	60	2016/09/19 – 2016/10/02	4032
Sensor	Occupancy	Zurich, CH	575	2015/10/26 – 2015/11/01	2016
Sensor	Speed	Birmingham, GB	4	2017/10/23 – 2017/11/18	7540
Sensor	Speed	Bolton, GB	16	2017/11/13 – 2017/11/18	1491
Sensor	Speed	Constance, DE	42	2017/02/13 – 2017/02/19	2015
Sensor	Speed	Essen, DE	15	2017/03/27 – 2017/09/30	54023
Sensor	Speed	Groningen, NL	8	2017/09/21 – 2017/10/06	4584
Sensor	Speed	Manchester, GB	29	2017/09/08 – 2017/11/18	20497
Sensor	Speed	Rotterdam, NL	70	2017/09/21 – 2017/11/02	12276
Sensor	Speed	Torino, IT	71	2016/09/26 – 2016/10/16	6048
Sensor	Speed	Guangzhou, CN	214	2016/08/01 – 2016/09/30	9216
Sensor	Bus Demand	Montevideo, UY	675	2020/10/01 – 2020/10/29	744

Table A.2 Pre-training Datasets Summary

Data Format	Domain Type	Spatial Region	# Spatial Location	Temporal Range	# Temporal Step
Grid	Taxi Demand	Chicago, US	77	2021/01/01 – 2021/12/31	17520
Grid	Traffic Speed	Zhengzhou, CN	676	2022/03/05 – 2022/04/05	1403
Grid	Traffic Speed	Hangzhou, CN	672	2022/03/05 – 2022/04/05	1403
Grid	Traffic Speed	Chengdu, CN	728	2022/03/05 – 2022/04/05	1403
Grid	Traffic Speed	Jinan, CN	579	2022/03/05 – 2022/04/05	1403
Grid	Traffic Index	Shenzhen, CN	627	2017/01/01 – 2018/02/28	17280
Grid	Traffic Index	Chengdu, CN	524	2018/01/01 – 2018/02/28	17280
Grid	Crowd	Nanjing, CN	320	2020/11/11 – 2021/05/31	6980
Grid	Cellular	Nanjing, CN	320	2020/11/11 – 2021/05/31	6980

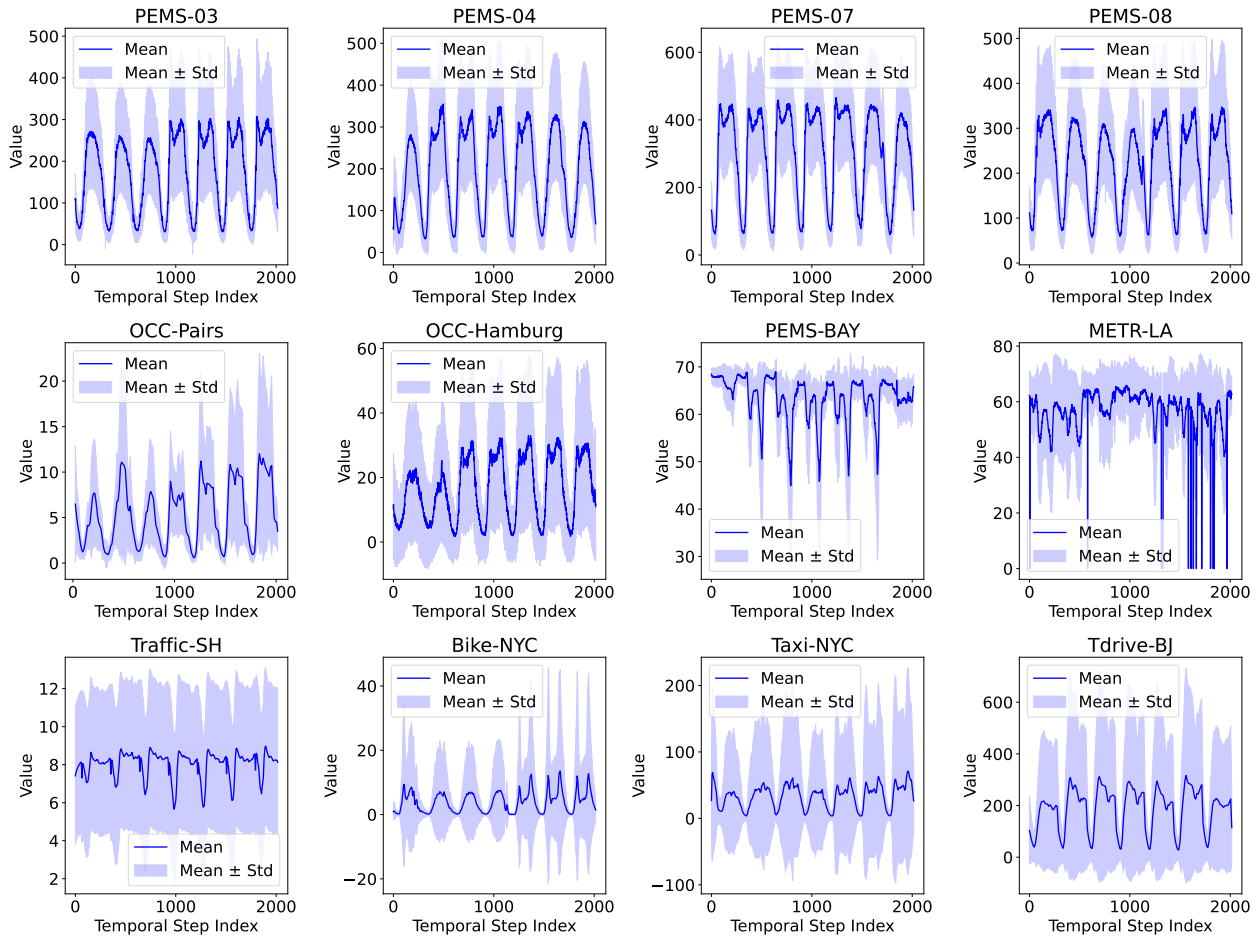


Figure A.2 Temporal Visualization of Eval1ST Benchmark.

B Method Detail

We first summarize the specific implementation details of our proposed Greedy Capacity-Constrained Clustering in Algorithm workflow 1. Furthermore, we provide schematic diagrams B.1 of clustering visualization effects under different capacities for two types of datasets: the sensor-based PEMS-08 and the grid-based Taxi-NYC.

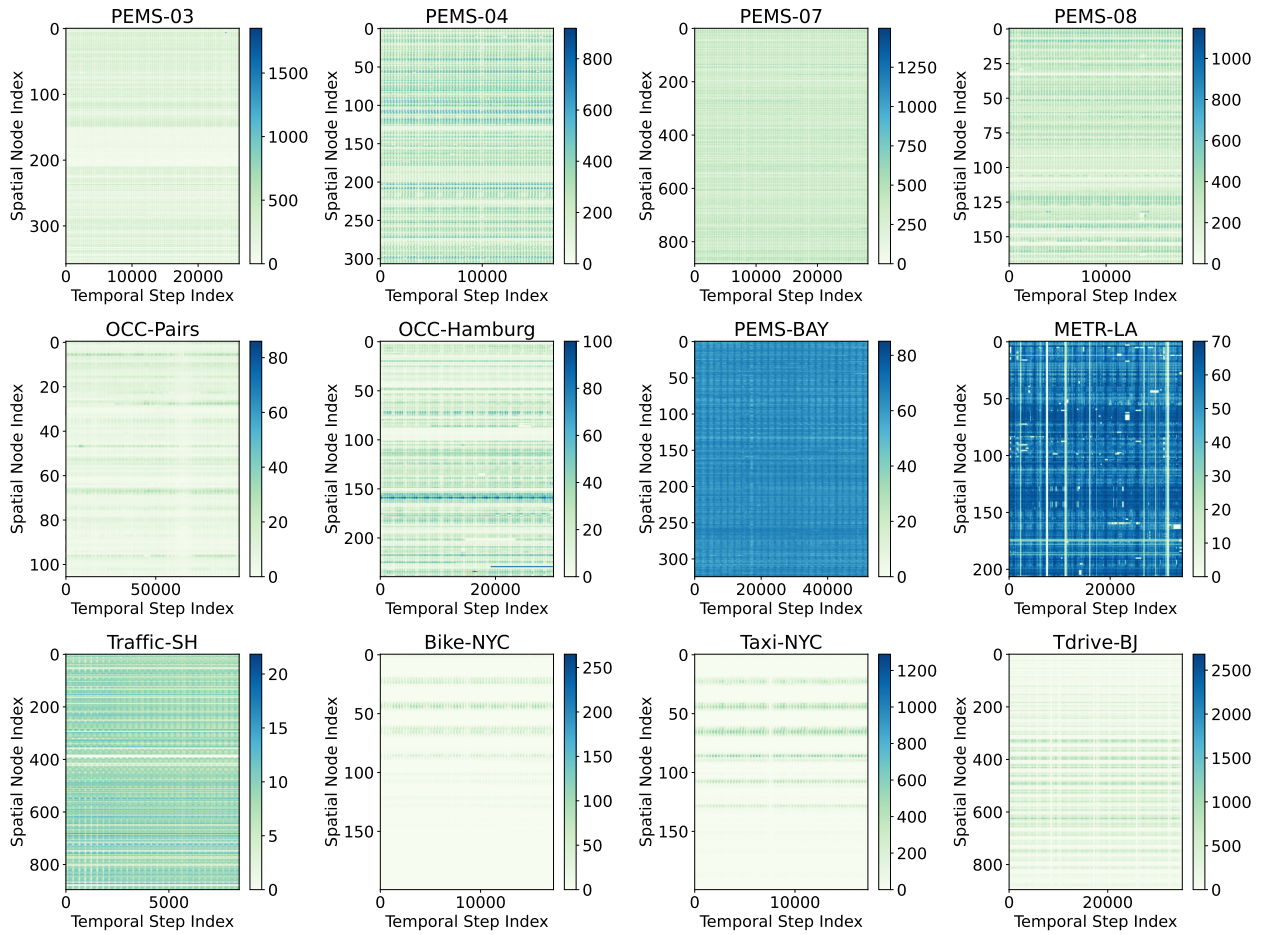


Figure A.3 Spatio-Temporal Visualization of EvalSTBenchmark.

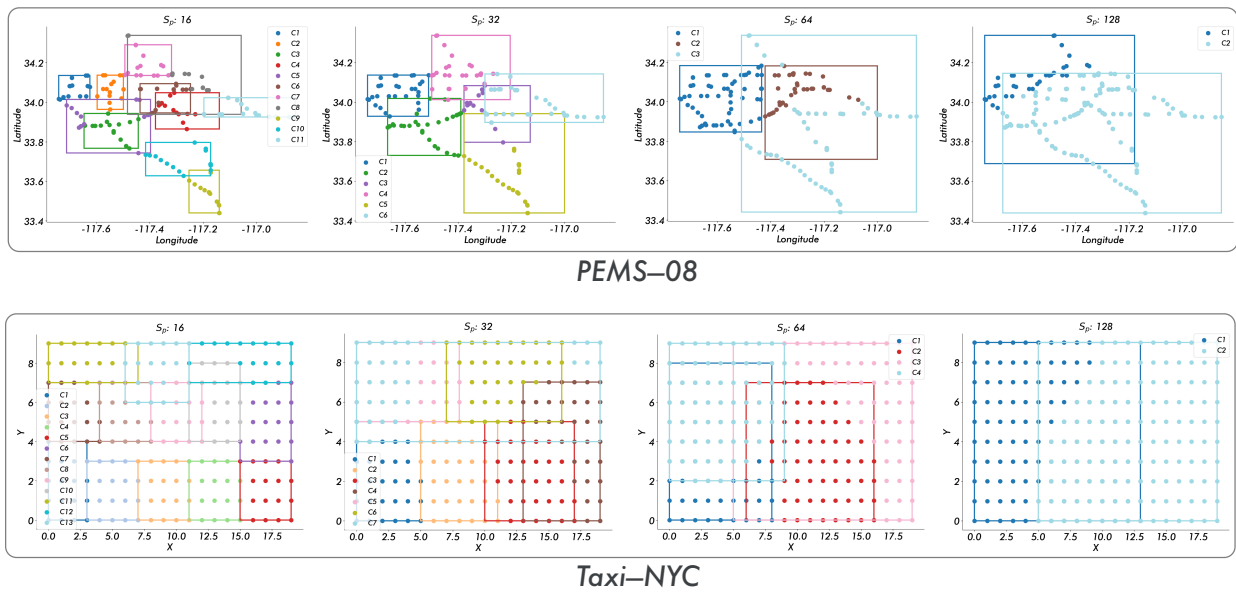


Figure B.1 Visualization of greedy capacity-constrained clustering with different S_p on PEMS-08 and Taxi-NYC.

Algorithm 1: Greedy Capacity-Constrained Clustering Algorithm Workflow.

Input : A set of points $P = \{p_1, \dots, p_n\}$; capacity parameter d
Output: Clusters C and corresponding index sets C_{idx}
 $n \leftarrow |P|$;
Build a KDTree T using the points in P ; Initialize $Assigned[1 \dots n] \leftarrow \text{False}$; $C, C_{idx} \leftarrow \emptyset$;
if $d \leq n$ then
 for $i \leftarrow 1$ to n do
 if $Assigned[i] = \text{False}$ then
 (distances, I) \leftarrow KDTreeQuery($T, p_i, k = d$);
 $cluster \leftarrow \emptyset, cluster_idx \leftarrow \emptyset$;
 foreach $idx \in I$ do
 if $Assigned[idx] = \text{False}$ then
 Add p_{idx} to $cluster$; Add idx to $cluster_idx$;
 if $|cluster| = d$ then
 break;
 end
 end
 end
 if $|cluster| < d$ then
 // If less than d points found, query all points
 (distances_{ext}, I_{ext}) \leftarrow KDTreeQuery($T, p_i, k = n$);
 foreach $idx \in I_{ext}$ do
 if $Assigned[idx] = \text{False}$ and $idx \notin cluster_idx$ then
 Add p_{idx} to $cluster$; Add idx to $cluster_idx$;
 if $|cluster| = d$ then
 break;
 end
 end
 end
 end
 foreach $idx \in cluster_idx$ do
 | $Assigned[idx] \leftarrow \text{True}$;
 end
 Append $cluster$ to C ; Append $cluster_idx$ to C_{idx} ;
 end
 end
 // Handle the last cluster if its size is less than d
 if $C \neq \emptyset$ and $|C[\text{last}]| < d$ then
 $last_c \leftarrow \text{last}(C); last_idx \leftarrow \text{last}(C_{idx}); needed \leftarrow d - |last_c|$;
 foreach $p \in last_c$ do
 (distances, I') \leftarrow KDTreeQuery($T, p, k = n$);
 foreach $idx \in I'$ do
 if $p_{idx} \notin last_c$ then
 Add p_{idx} to $last_c$; Add idx to $last_idx$; $needed \leftarrow needed - 1$;
 if $needed = 0$ then
 break;
 end
 end
 end
 if $needed = 0$ then
 break;
 end
 end
 $C[\text{last}] \leftarrow last_c; C_{idx}[\text{last}] \leftarrow last_idx$;
 end
end
else
 // Case when $d > n$: fill by repeating points
 $full \leftarrow \lfloor d/n \rfloor, rem \leftarrow d \bmod n$;
 for $j \leftarrow 1$ to $full$ do
 | Append P to C ; Append $\{1, \dots, n\}$ to C_{idx} ;
 end
 if $rem > 0$ then
 | Append first rem points of P to C ;
 | Append $\{1, \dots, rem\}$ to C_{idx} ;
 end
end
return C, C_{idx} ;

C Experimental Details

C.1 Baseline Details

In this appendix, we provide detailed descriptions of the expert and foundation baseline models used in our default evaluation.

C.1.1 Time Series Models

- *PatchTST* (Nie, 2022): *PatchTST* is a Transformer-based model that segments time series into sub-series patches. By leveraging patching and channel independence, it effectively reduces computational complexity while capturing both local semantic patterns and global long-term dependencies. <https://github.com/yuqinie98/PatchTST>
- *Dlinear* (Zeng et al., 2023): *Dlinear* is a simple yet robust baseline that decomposes time series into trend and remainder components. It models each component with a single-layer linear network, demonstrating that simple linear mappings can achieve high accuracy and robustness against distribution shifts. <https://github.com/cure-lab/LTSF-Linear>
- *LSTM* (Hochreiter and Schmidhuber, 1997): *LSTM* is a classic temporal modeling architecture designed to handle sequential dependencies. In the context of spatio-temporal learning, it serves as a fundamental building block for capturing non-linear temporal correlations and long-term trends across time steps. <https://github.com/liuxu77/LargeST/blob/main/src/models/lstm.py>
- *HA* (Cui et al., 2021): *HA* is a naive baseline that exploits the inherent historical inertia in time series data, directly utilizing the most recent input sequence as the prediction. https://github.com/GestaltCogTeam/BasicTS/blob/master/src/basicsts/models/HL/arch/hi_arch.py

C.1.2 ST-Grid Models

- *TAU* (Tan et al., 2023): *TAU* is a non-recurrent spatio-temporal model designed to parallelize the learning of temporal evolution. It introduces a novel attention mechanism that splits the temporal context into static (invariant) and dynamic (changing) components, allowing for effective global temporal modeling without the sequential constraints of RNNs. <https://github.com/chengtan9907/OpenSTL>
- *PredRNN++* (Wang et al., 2022): *PredRNN++* is a spatio-temporal recurrent network that introduces the Causal LSTM structure to cascade dual memory states and employs gradient highway units to enable efficient training across long sequences. <https://github.com/Yunbo426/predrnn-pp>
- *DSAN* (Lin et al., 2020): *DSAN* is a spatial-temporal forecasting framework designed to achieve effective long-term spatial-temporal prediction by filtering out spatial noise and alleviating long-term error propagation. <https://github.com/haoxing1/DSAN>
- *ST-ResNet* (Zhang et al., 2017): *ST-ResNet* is a grid-based spatial-temporal framework designed to model temporal closeness, period, and trend properties using three separate residual neural networks and aggregates them to capture citywide spatial-temporal dependencies. <https://github.com/topazape/ST-ResNet>

C.1.3 ST-Graph Models

- *STAEformer* (Liu et al., 2023): *STAEformer* is a spatial-temporal transformer architecture utilizing spatial-temporal adaptive embeddings to enhance representation learning for traffic forecasting tasks. <https://github.com/XDZhelheim/STAEformer>
- *STID* (Shao et al., 2022a): *STID* is a scalable model that addresses sample indistinguishability by introducing learnable spatial-temporal identity embeddings. These embeddings attach unique context

(e.g., time-of-day, sensor ID) to the input, enabling the efficient capture of node-specific dynamics. <https://github.com/GestaltCogTeam/STID>

- *D2STGNN* (Shao et al., 2022b): *D2STGNN* is a graph neural network that decouples spatial and temporal dependencies to prevent signal mixing. It utilizes separate graph convolution and recurrent modules to independently model diffusion signals and inherent traffic patterns for precise spatio-temporal forecasting. <https://github.com/GestaltCogTeam/D2STGNN>
- *GWNet* (Wu et al., 2019): *GWNet* is a spatial-temporal graph neural network that integrates diffusion graph convolutions with dilated causal temporal convolutions, utilizing a learnable self-adaptive adjacency matrix to capture latent spatial dependencies. <https://github.com/nanzhan/Graph-WaveNet>

C.1.4 Time Series Foundation Models

- *TimesFM++* (Das et al., 2024): *TimesFM++* is a large-scale pre-trained decoder-only foundation model developed by Google Research, capable of delivering high-accuracy univariate forecasting across diverse domains and frequencies. For this study, we utilize the *google/timesfm-2.0-500m-pytorch* checkpoint. <https://github.com/google-research/timesfm>
- *Moirai* (Woo et al., 2024): *Moirai* is a large-scale pre-trained encoder-only time series foundation model developed by Salesforce AI Research. It is specifically designed to deliver universal forecasting capabilities across diverse domains, frequencies, and variable types. For this study, we utilize the *moirai-1.0-R-base* checkpoint. <https://github.com/SalesforceAIResearch/uni2ts>
- *TimeMoE* (Shi et al., 2025): *TimeMoE* is a scalable forecasting foundation model leveraging a sparse Mixture-of-Experts (MoE) architecture. By dynamically activating only a subset of experts for each prediction, it significantly reduces inference costs while maintaining high model capacity. For this study, we utilize the *Maple728/TimeMoE-50M* checkpoints. <https://github.com/Time-MoE/Time-MoE>
- *Chronos* (Ansari et al., 2024): *Chronos* is a probabilistic time series foundation model that adapts the language modeling paradigm to the temporal domain. By tokenizing continuous values into a fixed vocabulary through scaling and quantization, it trains off-the-shelf Transformer architectures to learn universal temporal patterns from diverse datasets. For this study, we utilize the *amazon/chronos-bolt-base* checkpoints. <https://github.com/amazon-science/chronos-forecasting>

C.1.5 Spatio-Temporal Foundation Models

- *OpenCity* (Li et al., 2025): *OpenCity* is a spatial-temporal foundation model that supports zero-shot and few-shot forecasting across diverse city-level applications. For this study, we utilize the *Opencity-plus.pth* checkpoints. <https://github.com/HKUDS/OpenCity>
- *FactoST* (Zhong et al., 2026): *FactoST* is a factorized spatio-temporal foundation model that decouples universal temporal learning from domain-specific spatial adaptation, employing a minimalist temporal encoder and a lightweight spatial adapter to achieve efficient zero-shot and few-shot forecasting across diverse domains. For this study, we utilize the *factost_utp2_tiny_4sta.pt* checkpoints. <https://github.com/CityMind-Lab/FactoST>

C.1.6 Imputation Models

- *Mean*: *Mean* is a baseline imputation method that fills missing entries using the node-level average of the observed data.
- *KNN* (Crookston and Finley, 2008): *KNN* performs imputation by averaging the values of the $k = 10$ neighboring nodes with the highest weight in the adjacency matrix. <https://github.com/iskandr/fancyimpute>
- *MICE* (Van Buuren and Groothuis-Oudshoorn, 2011): *MICE* (Multivariate Imputation by Chained Equa-

tions) is a multiple imputation technique. For this study, the maximum number of iterations is limited to 100, and the number of nearest features is set to 10. https://github.com/Graph-Machine-Learning-Group/grin/blob/main/scripts/run_baselines.py

- *SVDImpute* (Xu et al., 2017): *SVDImpute* employs Singular Value Decomposition (SVD) to estimate missing values by iteratively refining the low-rank approximation of the data matrix to capture global spatial-temporal correlations. <https://github.com/iskandr/fancyimpute>

C.2 Details of Predefined Graph Construction

We follow conventional practices (Li et al., 2018) to define the graph topology based on the spatial distribution of sensors. Depending on the data structure, we employ two distinct strategies to construct the adjacency matrix: a distance-based threshold Gaussian kernel for station-based data, and a grid-based topology for raster data.

C.2.1 Distance-based Graph.

For irregularly distributed sensors (e.g., air quality and wind power datasets), we construct the adjacency matrix A using a threshold Gaussian kernel. Let d_{ij} denote the Haversine distance between sensor i and sensor j . The weighted adjacency matrix is defined as:

$$A_{ij} = \begin{cases} \exp\left(-\frac{d_{ij}^2}{\sigma^2}\right) & \text{if } \exp\left(-\frac{d_{ij}^2}{\sigma^2}\right) \geq r \quad \text{and} \quad i \neq j, \\ 0 & \text{otherwise,} \end{cases}$$

where σ is the standard deviation of distances between all valid sensor pairs, and r is the sparsity threshold. Empirically, we set r to 0.5 for the air quality dataset and 0.99 for the wind power dataset.

C.2.2 Grid-based Graph.

For datasets structured as a regular Euclidean grid (e.g., rasterized meteorological data), we define the graph topology using the Moore neighborhood (8-connectivity). Let (u_i, v_i) represent the grid coordinates (longitude and latitude indices) of node i . The binary adjacency matrix is constructed based on the first-order spatial proximity:

$$A_{ij} = \begin{cases} 1 & \text{if } |u_i - u_j| \leq 1 \quad \text{and} \quad |v_i - v_j| \leq 1 \quad \text{and} \quad i \neq j, \\ 0 & \text{otherwise.} \end{cases}$$

This ensures that each node is connected to its immediate spatial neighbors, including diagonals, while self-loops are excluded.

C.3 Protocol Details

C.3.1 Metrics Detail.

We use different metrics such as MAE, RMSE, MRE, and MAPE. Formally, these metrics are formulated as follows:

$$\text{MAE} = \frac{1}{n} \sum_{i=1}^n |y_i - \hat{y}_i|, \quad \text{RMSE} = \sqrt{\frac{1}{n} \sum_{i=1}^n (y_i - \hat{y}_i)^2}, \quad \text{MRE} = \frac{\sum_{i=1}^n |y_i - \hat{y}_i|}{\sum_{i=1}^n |y_i|}, \quad \text{MAPE} = \frac{100\%}{n} \sum_{i=1}^n \left| \frac{\hat{y}_i - y_i}{y_i} \right|,$$

where n represents the indices of all observed samples, y_i denotes the i -th actual sample and \hat{y}_i is the corresponding prediction.

C.3.2 Parameter Detail.

For all expert model baselines, hyper-parameters were set according to the recommendations of the corresponding papers and adjusted to achieve optimal results. The batch size was 128 by default; if it exceeded the

GPU memory, it was halved until it was completely unusable. For fair comparison, all models were trained for 100 epochs by default, and an early stopping strategy was used to prevent overfitting; that is, if the loss on the validation set did not improve for 10 consecutive epochs, training was stopped. For the foundation model baselines, we used the corresponding public checkpoints for testing. In addition, the fine-tuning phase uniformly used 10 epochs of full parameter fine-tuning. All experiments were conducted on a Linux server equipped with $(5 \times 1) \times$ Intel(R) Xeon(R) Gold 6248R CPU @ 3.00GHz (512GB memory) and $(5 \times 8) \times$ NVIDIA A100 (80GB memory) GPUs.

D More Experimental Results

D.1 More Result on Performance Evaluation

We provide complete experimental results on sensor-based and grid-based dataset benchmark, including the zero-shot of the foundation model compared with the few-shot of the expert model, and the few-shot of the foundation model compared with the full-shot of the expert model, which are presented in Table D.1, D.2, D.3, and D.4 respectively.

Table D.1 Comparison of the *zero-shot* results of the foundation models with the *few-shot* results of the expert models on the *short-term* (12 \rightarrow 12_{average}) and the *long-term* (24 \rightarrow 24_{average}) *forecasting* based on the grid dataset benchmark. ■ indicates best, ■ indicates second best.

Method Type		Zero-Shot of Foundation Model 🏠								Few-Shot (10% Training Set) of Expert Model 🏢											
		ST			TS					ST-Graph Method				ST-Grid Method				Time Series Method			
Method		UrbanFM	FactoST	OpenCity	TimesFM++	Moirai	TimeMoE	Chronos	STAEformer	STID	D2STGNN	GWNet	TAU	PredRNN++	DSAN	ST-ResNet	PatchTST	Dlinear	LSTM	HA	
Traffic-SH	Short	MAE	0.44	0.40	0.45	0.49	0.46	0.43	0.45	1.26 \pm 0.06	0.47 \pm 0.01	0.39 \pm 0.02	0.37 \pm 0.00	0.56 \pm 0.01	0.66 \pm 0.01	1.11 \pm 0.05	1.50 \pm 0.00	0.31 \pm 0.00	0.46 \pm 0.00	0.36 \pm 0.00	0.53 \pm 0.00
		RMSE	0.61	0.70	0.82	1.14	0.91	0.74	0.80	1.87 \pm 0.08	0.77 \pm 0.02	0.69 \pm 0.02	0.69 \pm 0.01	0.98 \pm 0.05	1.02 \pm 0.01	1.84 \pm 0.00	2.11 \pm 0.01	0.61 \pm 0.00	0.79 \pm 0.00	0.71 \pm 0.00	0.92 \pm 0.00
	Long	MAPE(%)	5.39	5.84	7.21	7.31	8.76	6.65	6.77	18.45 \pm 0.12	7.96 \pm 0.14	6.33 \pm 0.10	6.21 \pm 0.06	9.41 \pm 0.30	11.03 \pm 0.12	10.74 \pm 0.01	17.16 \pm 0.17	5.47 \pm 0.03	8.18 \pm 0.00	6.44 \pm 0.03	7.76 \pm 0.00
		MAE	0.49	0.58	0.48	0.65	0.66	0.60	0.67	2.94 \pm 0.52	0.60 \pm 0.01	0.56 \pm 0.02	0.68 \pm 0.01	0.70 \pm 0.03	0.80 \pm 0.03	1.21 \pm 0.00	1.54 \pm 0.01	0.48 \pm 0.00	0.59 \pm 0.00	0.51 \pm 0.00	0.53 \pm 0.00
	Long	RMSE	0.71	0.97	0.81	1.15	1.22	0.99	1.17	3.82 \pm 0.61	0.95 \pm 0.01	0.90 \pm 0.01	1.14 \pm 0.00	1.13 \pm 0.02	1.20 \pm 0.04	1.91 \pm 0.00	2.13 \pm 0.01	0.88 \pm 0.00	0.97 \pm 0.00	0.95 \pm 0.01	0.92 \pm 0.00
		MAPE(%)	6.23	9.30	7.41	10.16	12.72	9.57	9.99	40.09 \pm 7.07	10.24 \pm 0.05	9.45 \pm 0.29	11.81 \pm 0.17	11.25 \pm 0.45	13.49 \pm 0.64	12.29 \pm 0.01	17.98 \pm 0.09	8.62 \pm 0.00	10.74 \pm 0.01	9.58 \pm 0.08	7.76 \pm 0.00
Bike-NYC	Short	MAE	2.12	3.77	4.67	3.98	1.63	3.90	4.08	1.52 \pm 0.17	1.12 \pm 0.03	1.06 \pm 0.02	0.94 \pm 0.03	1.28 \pm 0.02	1.79 \pm 0.02	3.12 \pm 0.00	3.74 \pm 0.02	0.99 \pm 0.01	1.18 \pm 0.00	1.02 \pm 0.01	5.22 \pm 0.00
		RMSE	3.64	7.11	11.03	7.37	5.87	8.08	7.64	5.62 \pm 0.62	3.39 \pm 0.08	3.90 \pm 0.14	3.32 \pm 0.08	3.93 \pm 0.12	7.23 \pm 0.21	12.26 \pm 0.00	12.46 \pm 0.01	3.40 \pm 0.02	3.83 \pm 0.02	3.77 \pm 0.04	10.80 \pm 0.00
	Long	MAPE(%)	24.39	54.36	73.36	65.52	85.18	64.20	57.62	57.83 \pm 4.43	46.32 \pm 1.29	46.61 \pm 1.85	41.82 \pm 1.37	55.65 \pm 1.31	61.26 \pm 1.12	70.80 \pm 0.16	83.24 \pm 2.34	43.76 \pm 0.43	52.45 \pm 0.20	46.36 \pm 0.39	67.98 \pm 0.00
		MAE	2.81	5.89	5.17	5.74	2.67	5.52	6.17	2.44 \pm 0.38	1.59 \pm 0.01	1.44 \pm 0.01	1.71 \pm 0.03	1.60 \pm 0.00	1.93 \pm 0.04	3.25 \pm 0.00	3.85 \pm 0.08	1.69 \pm 0.01	1.77 \pm 0.00	1.63 \pm 0.07	5.18 \pm 0.00
	Long	RMSE	5.13	11.21	11.79	11.17	9.78	11.33	12.19	7.97 \pm 0.72	5.39 \pm 0.06	5.41 \pm 0.03	6.29 \pm 0.06	5.08 \pm 0.09	7.43 \pm 0.17	12.39 \pm 0.00	12.53 \pm 0.01	5.96 \pm 0.07	6.06 \pm 0.00	5.96 \pm 0.14	10.77 \pm 0.00
		MAPE(%)	29.53	75.63	85.08	92.49	134.82	83.27	87.06	99.60 \pm 21.14	56.47 \pm 0.59	55.85 \pm 0.62	66.85 \pm 0.48	63.65 \pm 0.75	68.35 \pm 0.86	80.26 \pm 0.08	86.39 \pm 1.40	65.15 \pm 0.60	70.93 \pm 0.40	65.76 \pm 1.13	67.38 \pm 0.00
Taxi-NYC	Short	MAE	5.60	8.84	12.23	8.95	7.58	10.05	9.48	8.60 \pm 0.54	6.18 \pm 0.41	5.34 \pm 0.21	5.04 \pm 0.09	6.59 \pm 0.12	10.80 \pm 0.17	22.56 \pm 0.01	24.04 \pm 0.05	4.08 \pm 0.01	4.77 \pm 0.00	4.86 \pm 0.06	18.83 \pm 0.00
		RMSE	11.65	21.68	41.34	20.04	22.72	23.50	21.69	27.34 \pm 1.58	15.29 \pm 0.40	16.17 \pm 0.23	16.67 \pm 0.06	19.01 \pm 0.59	35.48 \pm 0.76	78.95 \pm 0.00	79.20 \pm 0.03	12.34 \pm 0.04	13.66 \pm 0.01	15.85 \pm 0.21	52.17 \pm 0.00
	Long	MAPE(%)	29.55	42.33	53.82	49.50	63.33	89.85	43.22	61.05 \pm 2.76	106.73 \pm 25.20	49.62 \pm 8.52	44.47 \pm 2.06	68.53 \pm 0.78	74.84 \pm 5.67	55.68 \pm 0.21	122.35 \pm 5.68	36.24 \pm 0.28	39.47 \pm 0.28	39.96 \pm 0.32	72.60 \pm 0.00
		MAE	7.74	13.98	13.50	14.44	13.04	15.21	14.12	12.81 \pm 0.28	8.30 \pm 0.11	7.20 \pm 0.08	10.41 \pm 0.18	9.01 \pm 0.23	12.67 \pm 0.18	23.65 \pm 0.01	24.99 \pm 0.08	7.70 \pm 0.02	7.83 \pm 0.00	8.24 \pm 0.09	18.79 \pm 0.00
	Long	RMSE	16.33	33.21	40.83	33.44	40.13	37.26	33.02	40.60 \pm 1.45	23.44 \pm 0.25	24.28 \pm 0.43	32.32 \pm 0.48	26.81 \pm 0.56	39.88 \pm 0.99	79.90 \pm 0.01	80.07 \pm 0.03	23.65 \pm 0.12	23.67 \pm 0.01	26.36 \pm 0.15	52.16 \pm 0.00
		MAPE(%)	40.77	54.49	60.91	66.83	96.72	94.20	63.58	80.98 \pm 8.31	103.69 \pm 11.22	50.48 \pm 3.09	62.74 \pm 2.21	83.72 \pm 1.15	80.96 \pm 8.23	66.39 \pm 0.26	137.27 \pm 2.10	52.54 \pm 0.38	52.19 \pm 0.55	51.01 \pm 0.43	72.64 \pm 0.00
Thriving-BJ	Short	MAE	9.57	17.26	24.11	13.90	21.73	21.40	16.91	8.21 \pm 0.30	9.63 \pm 0.37	8.89 \pm 0.35	11.16 \pm 2.24	16.16 \pm 0.15	17.29 \pm 0.18	44.18 \pm 0.03	58.21 \pm 0.27	7.12 \pm 0.12	10.59 \pm 0.01	9.35 \pm 0.09	31.67 \pm 0.00
		RMSE	16.69	35.23	71.15	30.48	52.16	36.67	35.01	18.54 \pm 0.62	20.66 \pm 1.26	18.62 \pm 0.70	22.23 \pm 2.17	30.79 \pm 0.68	33.61 \pm 0.75	131.72 \pm 0.01	139.91 \pm 0.12	19.80 \pm 0.29	23.70 \pm 0.02	21.58 \pm 1.06	63.53 \pm 0.00
	Long	MAPE(%)	15.92	20.61	25.17	18.26	31.99	30.76	20.79	14.67 \pm 0.61	21.53 \pm 2.61	23.10 \pm 1.61	55.30 \pm 34.98	59.91 \pm 1.07	30.97 \pm 2.13	76.56 \pm 2.54	123.20 \pm 5.41	11.08 \pm 0.25	19.97 \pm 0.26	19.80 \pm 2.12	35.44 \pm 0.00
		MAE	12.92	26.28	50.05	29.89	38.79	30.94	27.54	20.48 \pm 0.41	19.56 \pm 0.08	15.52 \pm 0.40	22.89 \pm 0.31	26.23 \pm 1.05	25.33 \pm 0.51	49.94 \pm 0.02	60.27 \pm 0.19	18.52 \pm 0.08	21.72 \pm 0.04	16.44 \pm 0.18	31.69 \pm 0.00
	Long	RMSE	23.54	55.77	69.42	61.15	89.24	55.75	57.26	43.94 \pm 1.62	44.76 \pm 1.22	32.02 \pm 0.97	45.60 \pm 0.28	56.30 \pm 4.81	50.52 \pm 0.85	134.92 \pm 0.01	140.68 \pm 0.17	43.34 \pm 0.06	45.11 \pm 0.08	35.94 \pm 0.43	63.58 \pm 0.00
		MAPE(%)	20.62	31.31	30.96	40.51	56.76	57.15	34.69	39.76 \pm 20.85	30.34 \pm 2.96	25.10 \pm 1.87	53.90 \pm 0.60	86.47 \pm 1.45	39.13 \pm 2.50	82.85 \pm 1.27	128.38 \pm 1.40	25.15 \pm 0.01	35.17 \pm 0.90	27.40 \pm 1.50	35.49 \pm 0.00
1 st count		15	0	1	0	0	0	0	0	0	1	2	1	0	0	0	6	0	0	0	

D.2 More Result on Scaling Evaluation

We provide complete experimental results on the PEMS dataset benchmark, including the pre-trained data capacity of WorldST, the parameter capacity used by the UrbanFM model, and the partitioning parameters of MiniST. These results are presented in Tables D.5, D.6, D.7 and D.8.

E More Discussion

E.1 Ethics, Fairness, and Limitations

Despite the significant efforts we have made in this work, we still emphasize the following potential risks:

Table D.2 Comparison of the *zero-shot* results of the foundation models with the *few-shot* results of the expert models on the *short-term* (12 \rightarrow 12_{average}) and the *long-term* (24 \rightarrow 24_{average}) *forecasting* based on the *sensor* dataset benchmark. ■ indicates best, ■ indicates second best. OOM indicates Out-Of-Memory (NVIDIA A100-80G).

Method Type		Zero-Shot of Foundation Model								Few-Shot (10% Training Set) of Expert Model							
		ST			TS					ST-Graph Method				Time Series Method			
		UrbanFM	FactoST	OpenCity	TimesFM++	Moirai	TimeMoE	Chronos	STAEformer	STID	D2STGNN	GWNet	PatchTST	Dlinear	LSTM	HA	
PEMS-03	Short	MAE	15.62	25.84	25.57	27.13	29.02	29.12	26.48	20.07 \pm 0.39	17.88 \pm 0.12	17.78 \pm 0.17	17.96 \pm 0.68	21.04 \pm 0.07	21.17 \pm 0.00	19.08 \pm 0.38	32.01 \pm 0.00
		RMSE	23.24	40.26	49.25	40.94	44.11	43.36	41.10	32.35 \pm 0.38	28.50 \pm 0.31	29.56 \pm 0.59	28.82 \pm 0.89	32.92 \pm 0.09	33.26 \pm 0.01	31.04 \pm 0.71	55.52 \pm 0.00
		MAPE(%)	15.24	24.91	23.86	25.19	30.76	38.87	24.96	20.26 \pm 0.95	19.35 \pm 0.21	20.51 \pm 0.89	21.09 \pm 3.11	19.28 \pm 0.03	20.88 \pm 0.26	19.53 \pm 0.56	31.76 \pm 0.00
	Long	MAE	17.03	40.31	27.85	31.37	47.19	33.32	38.66	22.72 \pm 1.00	22.23 \pm 0.10	21.43 \pm 0.44	25.70 \pm 0.53	28.63 \pm 0.02	29.05 \pm 0.01	23.20 \pm 0.08	31.89 \pm 0.00
		RMSE	26.30	60.37	50.82	47.93	70.78	49.45	57.16	37.53 \pm 1.50	36.86 \pm 0.74	35.06 \pm 0.98	40.70 \pm 0.55	44.52 \pm 0.02	45.58 \pm 0.03	37.00 \pm 0.10	55.35 \pm 0.00
		MAPE(%)	15.96	41.07	27.95	32.20	57.64	48.53	40.87	22.68 \pm 1.20	24.32 \pm 0.82	23.17 \pm 1.16	28.09 \pm 2.55	25.98 \pm 0.02	29.42 \pm 0.21	23.64 \pm 0.46	31.68 \pm 0.00
PEMS-04	Short	MAE	20.95	33.07	32.82	33.11	37.15	36.62	34.13	31.85 \pm 4.72	24.61 \pm 0.14	23.95 \pm 0.21	26.78 \pm 1.33	27.37 \pm 0.04	27.54 \pm 0.00	26.02 \pm 0.19	39.00 \pm 0.00
		RMSE	32.21	48.33	58.42	48.55	54.41	53.71	50.45	46.48 \pm 5.88	37.44 \pm 0.17	37.05 \pm 0.37	40.69 \pm 1.41	42.39 \pm 0.01	42.63 \pm 0.01	39.81 \pm 0.29	65.02 \pm 0.00
		MAPE(%)	13.42	23.03	22.57	24.79	29.47	31.51	24.20	23.34 \pm 3.35	19.48 \pm 0.97	17.61 \pm 0.52	19.69 \pm 3.16	18.13 \pm 0.04	18.80 \pm 0.07	17.80 \pm 0.64	27.01 \pm 0.00
	Long	MAE	23.00	49.09	35.36	40.72	58.56	40.88	48.31	48.73 \pm 18.79	31.25 \pm 2.16	27.86 \pm 0.13	38.62 \pm 1.71	36.89 \pm 0.07	36.35 \pm 0.00	31.89 \pm 0.51	39.05 \pm 0.00
		RMSE	35.26	69.44	59.94	59.84	83.97	59.23	68.61	71.68 \pm 25.60	46.88 \pm 2.99	42.38 \pm 0.12	58.21 \pm 2.57	55.64 \pm 0.01	55.16 \pm 0.01	47.97 \pm 0.65	65.08 \pm 0.00
		MAPE(%)	15.03	38.10	26.28	27.69	55.67	35.86	38.79	42.39 \pm 23.54	27.43 \pm 4.50	19.28 \pm 0.72	29.42 \pm 3.12	24.85 \pm 0.09	26.13 \pm 0.17	22.40 \pm 0.49	27.02 \pm 0.00
PEMS-07	Short	MAE	23.71	38.06	34.50	38.47	42.76	40.28	39.73	25.72 \pm 0.32	25.88 \pm 0.61	25.39 \pm 0.13	26.98 \pm 0.43	30.65 \pm 0.12	31.22 \pm 0.03	27.99 \pm 0.22	38.96 \pm 0.00
		RMSE	34.99	56.47	58.19	56.15	62.20	58.42	58.54	40.05 \pm 0.51	39.41 \pm 0.52	39.02 \pm 0.08	41.13 \pm 0.40	46.75 \pm 0.14	47.30 \pm 0.05	42.59 \pm 0.34	68.31 \pm 0.00
		MAPE(%)	11.26	17.85	15.21	17.78	21.79	21.17	18.40	12.14 \pm 0.24	13.26 \pm 0.87	11.52 \pm 0.30	12.84 \pm 0.71	13.09 \pm 0.06	13.91 \pm 0.06	12.56 \pm 0.19	16.70 \pm 0.00
	Long	MAE	26.39	54.66	38.41	45.50	68.87	47.07	54.22	31.60 \pm 0.35	31.17 \pm 0.27	30.28 \pm 0.16	38.61 \pm 2.18	41.93 \pm 0.59	43.03 \pm 0.01	32.40 \pm 0.37	38.85 \pm 0.00
		RMSE	38.93	78.46	61.37	67.53	99.06	66.88	78.19	50.02 \pm 0.17	47.64 \pm 0.17	46.45 \pm 0.63	57.15 \pm 3.20	63.17 \pm 0.46	63.23 \pm 0.03	48.93 \pm 0.35	68.13 \pm 0.00
		MAPE(%)	12.09	26.76	17.91	19.94	40.56	26.83	27.17	15.77 \pm 0.25	16.14 \pm 0.47	14.70 \pm 1.46	19.66 \pm 1.92	18.50 \pm 0.21	21.28 \pm 0.10	14.63 \pm 0.42	16.65 \pm 0.00
PEMS-08	Short	MAE	17.70	27.60	26.92	27.43	30.93	29.63	28.25	32.73 \pm 9.30	19.68 \pm 0.21	19.92 \pm 0.36	20.93 \pm 0.62	22.10 \pm 0.13	22.34 \pm 0.01	20.28 \pm 0.10	33.36 \pm 0.00
		RMSE	25.80	40.22	47.47	40.11	45.60	42.64	41.82	48.59 \pm 14.23	30.56 \pm 0.42	30.90 \pm 0.62	32.42 \pm 0.54	34.38 \pm 0.16	34.47 \pm 0.01	31.73 \pm 0.07	58.70 \pm 0.00
		MAPE(%)	13.18	17.02	16.83	17.45	21.01	22.34	17.67	27.79 \pm 10.81	14.41 \pm 0.35	16.10 \pm 0.90	15.80 \pm 1.97	13.46 \pm 0.09	13.77 \pm 0.01	13.18 \pm 0.45	18.88 \pm 0.00
	Long	MAE	19.19	40.82	29.64	33.81	49.63	34.61	39.90	37.99 \pm 6.15	25.17 \pm 0.23	23.72 \pm 0.17	29.22 \pm 0.44	30.82 \pm 0.15	29.93 \pm 0.01	26.01 \pm 0.34	32.93 \pm 0.00
		RMSE	28.57	58.58	48.89	50.19	71.87	49.24	56.86	54.51 \pm 8.27	38.85 \pm 0.46	36.31 \pm 0.59	45.44 \pm 0.68	47.62 \pm 0.30	45.81 \pm 0.01	40.39 \pm 0.08	57.92 \pm 0.00
		MAPE(%)	13.77	26.89	19.50	21.09	37.59	31.37	26.56	37.66 \pm 13.00	17.58 \pm 0.24	18.69 \pm 1.68	19.35 \pm 1.02	18.65 \pm 0.09	18.46 \pm 0.08	17.81 \pm 1.50	18.72 \pm 0.00
OCC-Pairs	Short	MAE	0.71	1.33	1.80	1.43	1.60	1.81	1.29	0.94 \pm 0.01	0.88 \pm 0.01	0.99 \pm 0.01	0.96 \pm 0.02	1.05 \pm 0.00	1.05 \pm 0.00	0.97 \pm 0.02	2.38 \pm 0.00
		RMSE	1.66	2.89	3.99	3.15	3.39	3.47	2.88	2.58 \pm 0.07	2.31 \pm 0.03	2.57 \pm 0.05	2.41 \pm 0.05	2.66 \pm 0.00	2.62 \pm 0.00	2.45 \pm 0.03	5.14 \pm 0.00
		MAPE(%)	10.45	22.71	35.19	26.17	32.78	64.49	23.82	15.02 \pm 0.17	13.72 \pm 0.35	15.96 \pm 1.44	16.41 \pm 0.57	18.04 \pm 0.06	19.06 \pm 0.07	16.31 \pm 0.64	37.53 \pm 0.00
	Long	MAE	1.00	1.97	2.03	1.99	2.56	2.13	2.00	1.42 \pm 0.03	1.39 \pm 0.01	1.45 \pm 0.01	1.88 \pm 0.03	1.70 \pm 0.00	1.69 \pm 0.00	1.40 \pm 0.01	2.38 \pm 0.00
		RMSE	2.13	3.83	4.14	3.88	4.91	3.99	3.92	3.25 \pm 0.07	3.17 \pm 0.05	3.29 \pm 0.05	3.86 \pm 0.05	3.58 \pm 0.00	3.53 \pm 0.00	3.11 \pm 0.01	5.14 \pm 0.00
		MAPE(%)	14.70	39.55	43.62	40.41	62.44	64.83	38.82	23.52 \pm 0.80	21.29 \pm 0.30	23.71 \pm 0.69	31.16 \pm 1.04	30.26 \pm 0.06	32.15 \pm 0.08	23.00 \pm 0.88	37.55 \pm 0.00
OCC-Hamburg	Short	MAE	6.06	6.62	7.07	6.84	7.53	8.14	6.80	6.05 \pm 0.01	5.99 \pm 0.02	6.10 \pm 0.02	5.95 \pm 0.02	6.28 \pm 0.00	6.32 \pm 0.00	5.93 \pm 0.02	8.82 \pm 0.00
		RMSE	10.04	10.95	11.41	11.27	12.51	12.84	11.27	10.34 \pm 0.01	10.16 \pm 0.08	10.31 \pm 0.04	10.09 \pm 0.05	10.62 \pm 0.00	10.57 \pm 0.00	10.09 \pm 0.02	15.32 \pm 0.00
		MAPE(%)	48.99	89.77	132.37	89.72	130.17	161.98	88.85	79.72 \pm 2.59	79.58 \pm 0.24	83.33 \pm 2.36	77.64 \pm 1.52	84.02 \pm 0.03	88.49 \pm 0.10	76.91 \pm 1.19	119.15 \pm 0.00
	Long	MAE	6.05	7.87	7.33	7.84	8.99	8.56	7.86	6.40 \pm 0.07	6.33 \pm 0.04	6.32 \pm 0.03	6.61 \pm 0.05	6.90 \pm 0.01	7.00 \pm 0.00	6.22 \pm 0.01	8.81 \pm 0.00
		RMSE	10.05	12.64	11.68	12.85	14.48	13.49	12.67	11.02 \pm 0.08	10.88 \pm 0.18	10.90 \pm 0.03	11.02 \pm 0.10	11.51 \pm 0.02	11.55 \pm 0.00	10.55 \pm 0.02	15.31 \pm 0.00
		MAPE(%)	48.33	117.38	143.16	109.41	171.8	170.60	112.93	86.61 \pm 5.63	86.19 \pm 0.42	88.54 \pm 1.52	93.71 \pm 4.05	94.20 \pm 0.42	101.48 \pm 0.43	79.98 \pm 0.66	118.99 \pm 0.00
PEMS-Bay	Short	MAE	1.68	2.21	2.22	2.49	2.58	2.42	2.45	1.85 \pm 0.01	1.84 \pm 0.00	1.83 \pm 0.02	1.88 \pm 0.01	2.07 \pm 0.00	2.14 \pm 0.00	1.93 \pm 0.03	3.57 \pm 0.00
		RMSE	3.27	4.96	4.71	5.71	6.11	5.01	5.46	4.03 \pm 0.01	4.00 \pm 0.01	4.02 \pm 0.03	4.20 \pm 0.02	4.82 \pm 0.00	4.79 \pm 0.00	4.32 \pm 0.06	6.67 \pm 0.00
		MAPE(%)	3.46	4.88	5.23	5.85	6.26	6.02	5.42	4.28 \pm 0.03	4.28 \pm 0.00	4.26 \pm 0.04	4.31 \pm 0.03	4.52 \pm 0.01	4.86 \pm 0.00	4.40 \pm 0.07	8.22 \pm 0.00
	Long	MAE	2.11	3.35	2.68	3.41	3.84	3.10	3.25	2.30 \pm 0.01	2.26 \pm 0.00	2.21 \pm 0.01	2.69 \pm 0.03	2.88 \pm 0.00	2.87 \pm 0.00	2.41 \pm 0.01	3.57 \pm 0.00
		RMSE	4.19	7.26	5.70	7.57	8.53	6.50	7.26	4.90 \pm 0.02	4.82 \pm 0.01	4.82 \pm 0.01	5.80 \pm 0.06	6.52 \pm 0.01	6.30 \pm 0.00	5.34 \pm 0.03	6.68 \pm 0.00
		MAPE(%)	4.52	7.71	6.56	8.10	9.77	8.20	7.28	5.56 \pm 0.05	5.50 \pm 0.07	5.35 \pm 0.07	6.76 \pm 0.12	6.71 \pm 0.04	7.08 \pm 0.01	6.05 \pm 0.09	8.23 \pm 0.00
METR-LA	Short	MAE	4.23	5.19	5.44	5.06	6.41	5.53	5.63								

Table D.3 Comparison of the *few-shot* results of the foundation models with the *full-shot* results of the expert models on the *short-term* (12 \rightarrow 12_{average}) and the *long-term* (24 \rightarrow 24_{average}) *forecasting* based on the sensor dataset benchmark. indicates best, indicates second best.

Method Type		Few-Shot (10% Training Set) of Foundation Model								Full-Shot of Expert Model							
		ST			TS					ST-Graph Method				Time Series Method			
		Model	UrbanFM	FactoST	OpenCity	TimesFM++	Moirai	TimeMoE	Chronos	STAEformer	STID	D2STGNN	GWNet	PatchTST	Dlinear	LSTM	HA
PEMS-03	Short	MAE	13.00	21.08	16.91	21.56	20.54	20.59	21.31	15.13\pm0.10	15.21\pm0.03	14.88 \pm 0.11	14.91 \pm 0.12	20.84 \pm 0.01	21.04 \pm 0.00	16.69 \pm 0.06	26.17 \pm 0.00
		RMSE	19.87	32.88	27.18	33.72	31.68	31.98	33.72	26.84\pm0.56	25.52\pm0.28	25.76 \pm 0.23	25.82 \pm 0.30	32.57 \pm 0.02	33.08 \pm 0.02	28.21 \pm 0.20	47.52 \pm 0.00
		MAPE(%)	12.43	19.28	18.57	19.61	19.63	22.11	19.21	15.33\pm0.12	16.36\pm0.13	15.02\pm0.28	15.19 \pm 0.42	19.13 \pm 0.03	20.78 \pm 0.09	16.05 \pm 0.27	26.89 \pm 0.00
	Long	MAE	13.82	28.62	19.29	30.08	28.74	26.59	29.81	17.30 \pm 0.34	17.07 \pm 0.06	16.45\pm0.09	20.37\pm0.39	27.84 \pm 0.14	28.66 \pm 0.00	19.57 \pm 0.03	26.19 \pm 0.00
		RMSE	21.24	44.65	32.26	46.86	44.73	40.86	47.91	30.62\pm0.85	29.34\pm0.24	28.52 \pm 0.13	33.93\pm0.77	43.49 \pm 0.22	44.98 \pm 0.03	32.77 \pm 0.10	47.56 \pm 0.00
		MAPE(%)	12.89	25.96	21.19	26.93	26.13	29.98	26.64	17.37 \pm 0.14	18.21 \pm 0.12	16.50\pm0.29	20.30\pm0.54	25.48 \pm 0.20	28.70 \pm 0.64	18.70 \pm 0.65	26.91 \pm 0.00
PEMS-04	Short	MAE	18.72	27.39	23.43	27.98	26.85	26.46	28.22	18.29\pm0.05	18.53\pm0.05	19.08 \pm 0.06	18.80 \pm 0.18	27.02 \pm 0.05	27.24 \pm 0.00	22.89 \pm 0.25	26.35 \pm 0.00
		RMSE	29.58	42.25	36.61	42.92	41.01	40.22	44.26	30.48\pm0.27	30.37\pm0.07	30.95 \pm 0.08	30.74 \pm 0.25	42.03 \pm 0.05	30.29\pm0.17	36.23 \pm 0.28	42.16 \pm 0.00
		MAPE(%)	12.19	18.08	17.90	18.59	18.41	19.34	18.35	12.09\pm0.06	12.37\pm0.15	12.76 \pm 0.14	12.56 \pm 0.21	17.96 \pm 0.06	18.69 \pm 0.10	15.27 \pm 0.26	16.74 \pm 0.00
	Long	MAE	19.78	36.69	29.33	38.44	37.16	34.12	38.22	19.25 \pm 0.04	19.97 \pm 0.09	19.93 \pm 0.02	23.94 \pm 0.18	35.32 \pm 0.11	35.74 \pm 0.00	26.33 \pm 0.09	26.38 \pm 0.00
		RMSE	30.87	56.08	45.66	57.89	56.05	51.11	59.87	32.06\pm0.12	32.47\pm0.12	32.68 \pm 0.12	37.80 \pm 0.16	54.44 \pm 0.04	54.30 \pm 0.05	41.39 \pm 0.09	42.20 \pm 0.00
		MAPE(%)	12.83	24.81	25.13	26.01	25.15	25.00	25.58	12.60\pm0.07	13.58\pm0.21	13.08 \pm 0.04	16.30 \pm 0.30	23.75 \pm 0.10	26.15 \pm 0.19	18.05 \pm 0.23	16.73 \pm 0.00
PEMS-07	Short	MAE	19.45	29.70	25.16	31.62	28.91	31.62	31.40	19.53\pm0.08	19.71\pm0.03	20.05 \pm 0.07	20.70\pm0.49	29.19 \pm 0.02	30.81 \pm 0.00	23.84 \pm 0.24	30.32 \pm 0.00
		RMSE	30.32	46.75	40.51	48.15	44.02	48.15	48.80	33.26\pm0.02	32.74\pm0.04	33.10 \pm 0.06	33.71 \pm 0.44	45.75 \pm 0.05	46.96 \pm 0.02	38.00 \pm 0.22	56.67 \pm 0.00
		MAPE(%)	8.14	12.64	11.07	13.31	12.48	13.31	13.12	8.25\pm0.05	8.37\pm0.03	8.59 \pm 0.14	8.86\pm0.28	12.47 \pm 0.00	13.43 \pm 0.02	9.99 \pm 0.18	12.80 \pm 0.00
	Long	MAE	21.12	39.99	28.71	45.91	21.50	OOM	44.70	21.25 \pm 0.04	21.44 \pm 0.09	21.30 \pm 0.19	27.50 \pm 0.05	38.79 \pm 0.09	42.16 \pm 0.01	27.50 \pm 0.04	30.33 \pm 0.00
		RMSE	32.93	63.60	47.38	67.28	33.16	OOM	72.43	36.64\pm0.06	35.65\pm0.12	35.52\pm0.25	43.11 \pm 0.19	60.64 \pm 0.16	62.44 \pm 0.02	43.87 \pm 0.04	56.68 \pm 0.00
		MAPE(%)	9.49	17.57	13.09	21.07	13.61	OOM	20.17	9.06\pm0.04	9.31 \pm 0.10	9.36 \pm 0.13	12.56 \pm 0.08	17.16 \pm 0.05	19.74 \pm 0.24	11.92 \pm 0.18	12.79 \pm 0.00
PEMS-08	Short	MAE	14.34	21.98	21.53	22.66	30.88	21.18	22.60	13.53\pm0.05	14.23\pm0.02	14.47 \pm 0.07	14.90 \pm 0.11	20.24 \pm 0.01	21.87 \pm 0.01	17.00 \pm 0.03	23.30 \pm 0.00
		RMSE	22.25	34.64	34.77	35.28	47.40	32.66	35.82	23.25\pm0.08	23.30\pm0.05	23.63 \pm 0.16	23.84 \pm 0.20	32.69 \pm 0.01	33.80 \pm 0.02	27.29 \pm 0.03	40.58 \pm 0.00
		MAPE(%)	8.87	13.25	13.03	13.72	18.64	14.39	13.64	9.02\pm0.03	9.38\pm0.06	9.59 \pm 0.23	10.16 \pm 0.20	12.52 \pm 0.01	13.63 \pm 0.06	10.81 \pm 0.17	14.49 \pm 0.00
	Long	MAE	15.56	29.92	25.13	31.77	30.88	OOM	32.11	14.71\pm0.03	15.52\pm0.02	15.44 \pm 0.03	19.52 \pm 0.04	26.34 \pm 0.09	28.90 \pm 0.01	19.16 \pm 0.06	23.32 \pm 0.00
		RMSE	24.27	47.78	34.77	48.34	47.40	OOM	55.25	25.58\pm0.12	25.44\pm0.03	25.79 \pm 0.22	30.76 \pm 0.05	42.29 \pm 0.19	43.93 \pm 0.01	30.75 \pm 0.07	40.62 \pm 0.00
		MAPE(%)	9.89	18.28	13.03	19.18	18.64	OOM	19.49	9.84\pm0.05	10.48\pm0.14	10.28 \pm 0.09	12.93 \pm 0.10	16.38 \pm 0.07	18.30 \pm 0.07	12.39 \pm 0.04	14.48 \pm 0.00
OCC-Pairs	Short	MAE	0.33	1.04	1.01	1.06	1.00	1.02	1.34	0.72\pm0.00	0.72\pm0.00	0.83 \pm 0.01	0.75 \pm 0.00	1.04 \pm 0.00	1.04 \pm 0.00	0.86 \pm 0.00	1.86 \pm 0.00
		RMSE	1.29	2.66	2.34	2.66	2.57	2.60	3.73	1.98\pm0.01	1.98\pm0.00	2.09 \pm 0.02	2.02 \pm 0.03	2.65 \pm 0.00	2.61 \pm 0.00	2.30 \pm 0.01	3.96 \pm 0.00
		MAPE(%)	4.80	17.97	19.56	18.36	17.36	17.50	22.65	11.12\pm0.12	11.30\pm0.09	13.59 \pm 0.67	11.71 \pm 0.15	18.11 \pm 0.04	18.99 \pm 0.03	14.11 \pm 0.03	33.36 \pm 0.00
	Long	MAE	0.46	1.69	1.36	1.95	1.71	OOM	1.85	1.09 \pm 0.01	1.09\pm0.01	1.14 \pm 0.02	1.47 \pm 0.00	1.69 \pm 0.00	1.67 \pm 0.00	1.27 \pm 0.01	1.87 \pm 0.00
		RMSE	1.43	3.58	2.87	3.86	3.58	OOM	3.88	2.48\pm0.02	2.52\pm0.02	2.59 \pm 0.05	3.06 \pm 0.01	3.57 \pm 0.00	3.48 \pm 0.00	2.89 \pm 0.02	3.96 \pm 0.00
		MAPE(%)	6.16	29.94	27.26	37.11	30.30	OOM	32.15	18.05\pm0.50	17.27\pm0.21	18.58 \pm 0.68	25.38 \pm 0.18	30.46 \pm 0.14	32.42 \pm 0.22	20.37 \pm 0.14	33.37 \pm 0.00
OCC-Hamburg	Short	MAE	5.74	6.51	6.05	6.59	6.49	6.51	6.60	5.73\pm0.05	5.74\pm0.01	5.87 \pm 0.02	5.73\pm0.03	6.27 \pm 0.00	6.29 \pm 0.00	5.83 \pm 0.01	7.03 \pm 0.00
		RMSE	9.52	10.74	9.97	10.85	10.67	10.69	11.01	9.92 \pm 0.16	9.92 \pm 0.04	10.34 \pm 0.18	9.83\pm0.07	10.60 \pm 0.00	10.51 \pm 0.00	9.99 \pm 0.01	12.66 \pm 0.00
		MAPE(%)	45.91	91.63	92.50	89.68	94.29	108.86	81.08	72.98\pm3.54	72.93\pm0.96	76.28 \pm 0.40	74.30 \pm 1.01	84.64 \pm 0.59	88.69 \pm 0.27	75.45 \pm 0.77	107.48 \pm 0.00
	Long	MAE	5.77	7.14	6.29	7.43	7.14	7.19	7.35	5.86\pm0.01	5.85\pm0.00	6.02 \pm 0.01	6.24 \pm 0.02	6.88 \pm 0.00	6.96 \pm 0.00	6.09 \pm 0.01	7.03 \pm 0.00
		RMSE	9.57	11.61	10.31	12.09	11.63	11.70	12.15	10.05\pm0.04	10.11\pm0.03	10.62 \pm 0.02	10.84 \pm 0.13	11.49 \pm 0.01	11.47 \pm 0.00	10.37 \pm 0.02	12.65 \pm 0.00
		MAPE(%)	46.63	107.30	101.77	104.72	105.08	117.74	96.51	81.32\pm2.33	73.89\pm0.46	80.25 \pm 0.89	82.08 \pm 0.36	93.49 \pm 0.66	101.38 \pm 0.46	78.78 \pm 0.96	107.32 \pm 0.00
PEMS-Bay	Short	MAE	1.08	2.06	1.93	2.36	2.02	2.02	2.10	1.58\pm0.01	1.61 \pm 0.00	1.60 \pm 0.01	1.63 \pm 0.00	2.07 \pm 0.00	2.13 \pm 0.00	1.80 \pm 0.00	2.70 \pm 0.00
		RMSE	2.15	4.78	4.19	5.18	4.60	4.55	4.83	3.57\pm0.00	3.61 \pm 0.00	3.60 \pm 0.03	3.66 \pm 0.01	4.81 \pm 0.00	4.77 \pm 0.01	4.07 \pm 0.01	5.33 \pm 0.00
		MAPE(%)	2.18	4.49	4.36	5.00	4.48	4.65	4.62	3.57\pm0.03	3.60 \pm 0.02	3.61 \pm 0.08	3.66 \pm 0.03	4.52 \pm 0.01	4.84 \pm 0.00	4.15 \pm	

Table D.4 Comparison of the *few-shot* results of the foundation models with the *full-shot* results of the expert models on the *short-term* (12 \rightarrow 12_{average}) and the *long-term* (24 \rightarrow 24_{average}) forecasting based on the grid dataset benchmark. ● indicates best, ● indicates second best.

Method Type	Few-Shot (10% Training Set) of Foundation Model							Full-Shot of Expert Model												
	ST			TS				ST-Graph Method			ST-Grid Method			Time Series Method						
	Method	UrbanFM	FactoST	OpenCity	TimesFM++	Moirai	TimeMoE	Chronos	STAEformer	STID	D2STGNN	GWNet	TAU	PredRNN++	DSAN	ST-ResNet	PatchTST	Dlinear	LSTM	HA
Traffic-SH	MAE	0.10	0.34	0.44	0.39	0.34	OOM	0.34	0.24\pm0.00	0.25\pm0.01	0.24\pm0.00	0.27\pm0.01	0.40 \pm 0.00	0.32 \pm 0.00	1.04 \pm 0.00	1.09 \pm 0.00	0.30 \pm 0.00	0.43 \pm 0.00	0.31 \pm 0.00	0.92 \pm 0.00
	Short RMSE	0.26	0.62	0.77	0.69	0.62	OOM	0.64	0.57 \pm 0.00	0.50\pm0.01	0.56\pm0.02	0.56\pm0.02	0.74 \pm 0.01	0.62 \pm 0.00	1.80 \pm 0.00	1.80 \pm 0.00	0.61 \pm 0.00	0.76 \pm 0.00	0.62 \pm 0.01	1.22 \pm 0.00
	MAPE(%)	1.47	5.25	7.33	6.14	5.31	OOM	5.29	4.41 \pm 0.00	4.23\pm0.08	4.38 \pm 0.08	4.78 \pm 0.18	6.86 \pm 0.05	5.65 \pm 0.09	9.58 \pm 0.01	10.70 \pm 0.04	5.34 \pm 0.05	7.72 \pm 0.02	5.57 \pm 0.06	12.76 \pm 0.00
Bike-NYC	MAE	0.20	0.54	0.48	0.57	OOM	OOM	0.55	0.33 \pm 0.00	0.35 \pm 0.00	0.32\pm0.00	0.48 \pm 0.01	0.44 \pm 0.01	0.41 \pm 0.01	1.16 \pm 0.00	1.13 \pm 0.01	0.47 \pm 0.00	0.56 \pm 0.00	0.41 \pm 0.00	0.93 \pm 0.00
	Short RMSE	0.40	0.91	0.78	0.95	OOM	OOM	0.94	0.66 \pm 0.01	0.66 \pm 0.02	0.64\pm0.01	0.89\pm0.03	0.78 \pm 0.01	0.76 \pm 0.01	1.88 \pm 0.00	1.82 \pm 0.00	0.88 \pm 0.00	0.94 \pm 0.00	0.76 \pm 0.00	1.23 \pm 0.00
	MAPE(%)	2.78	8.54	7.58	9.07	OOM	OOM	8.63	5.83 \pm 0.04	6.01 \pm 0.06	5.73\pm0.07	8.48 \pm 0.26	7.39 \pm 0.10	7.28 \pm 0.13	11.45 \pm 0.01	11.26 \pm 0.11	8.46 \pm 0.05	10.27 \pm 0.02	7.45 \pm 0.08	12.82 \pm 0.00
Taxi-NYC	MAE	0.73	3.05	3.58	3.22	3.00	3.18	3.32	0.61\pm0.01	0.64\pm0.01	0.64\pm0.01	0.61\pm0.01	0.81 \pm 0.01	1.00 \pm 0.01	2.66 \pm 0.00	2.70 \pm 0.01	0.95 \pm 0.01	1.07 \pm 0.00	0.74 \pm 0.01	3.68 \pm 0.00
	Short RMSE	1.46	5.89	7.33	6.16	5.87	7.12	6.51	1.86 \pm 0.01	1.93 \pm 0.04	1.99 \pm 0.04	1.89\pm0.02	2.31 \pm 0.01	3.33 \pm 0.14	11.20 \pm 0.00	11.17 \pm 0.00	3.21 \pm 0.02	3.40 \pm 0.00	2.33 \pm 0.05	6.77 \pm 0.00
	MAPE(%)	9.11	43.86	65.40	50.27	43.20	43.18	45.85	33.33 \pm 0.43	32.69 \pm 0.17	33.26 \pm 1.05	31.94\pm0.23	39.05 \pm 0.33	45.65 \pm 0.85	62.57 \pm 0.16	57.51 \pm 0.32	43.97 \pm 0.47	49.77 \pm 0.16	37.91 \pm 0.75	55.02 \pm 0.00
Drive-BJ	MAE	1.55	5.22	4.76	5.70	5.27	OOM	5.42	0.90 \pm 0.01	0.85\pm0.01	0.84\pm0.02	1.08 \pm 0.01	0.97 \pm 0.00	1.12 \pm 0.01	2.87 \pm 0.00	2.77 \pm 0.05	1.56 \pm 0.00	1.65 \pm 0.00	1.01 \pm 0.00	3.69 \pm 0.00
	Short RMSE	2.83	10.42	10.12	11.27	10.44	OOM	11.13	2.69 \pm 0.03	2.60\pm0.05	2.56\pm0.06	3.40 \pm 0.05	2.81 \pm 0.04	3.60 \pm 0.08	11.37 \pm 0.00	11.23 \pm 0.01	5.31 \pm 0.02	5.54 \pm 0.00	3.19 \pm 0.02	6.78 \pm 0.00
	MAPE(%)	18.17	65.67	76.80	72.42	64.14	OOM	66.84	45.35 \pm 0.70	40.64 \pm 0.17	43.38 \pm 2.37	50.47 \pm 1.04	46.85 \pm 0.61	50.08 \pm 1.00	75.22 \pm 0.31	58.13 \pm 0.74	63.92 \pm 0.42	71.63 \pm 0.48	48.91 \pm 0.73	55.03 \pm 0.00
1 st count	MAE	2.19	6.40	8.07	9.32	6.25	6.98	7.01	2.50\pm0.07	2.63 \pm 0.06	2.66 \pm 0.17	2.64 \pm 0.07	3.34 \pm 0.02	3.96 \pm 0.04	20.06 \pm 0.00	19.39 \pm 0.01	3.99 \pm 0.00	4.23 \pm 0.01	3.57 \pm 0.11	9.55 \pm 0.00
	Short RMSE	4.98	15.47	19.28	20.90	15.09	19.73	17.46	6.73 \pm 0.20	6.98 \pm 0.22	7.20 \pm 0.47	7.10 \pm 0.21	8.32 \pm 0.08	12.08 \pm 0.28	73.55 \pm 0.00	73.17 \pm 0.00	11.99 \pm 0.03	12.17 \pm 0.01	10.14 \pm 0.41	22.68 \pm 0.00
	MAPE(%)	13.06	36.42	48.12	37.24	32.93	35.15	32.71	27.09 \pm 0.34	28.96 \pm 0.25	28.34 \pm 1.65	28.78 \pm 0.43	39.61 \pm 0.28	37.84 \pm 1.19	50.00 \pm 0.11	50.37 \pm 0.85	35.92 \pm 0.17	37.53 \pm 0.19	32.60 \pm 0.58	42.33 \pm 0.00
1 st count	MAE	3.37	12.26	11.22	12.70	12.24	OOM	12.85	3.51 \pm 0.02	3.58 \pm 0.06	3.58 \pm 0.06	4.91 \pm 0.04	4.11 \pm 0.03	4.61 \pm 0.02	21.46 \pm 0.02	19.63 \pm 0.02	7.35 \pm 0.01	7.20 \pm 0.01	5.14 \pm 0.03	9.55 \pm 0.00
	Long RMSE	7.78	30.06	27.07	30.48	29.75	OOM	32.11	9.58 \pm 0.15	9.77 \pm 0.15	9.79 \pm 0.26	14.10 \pm 0.17	10.89 \pm 0.12	14.40 \pm 0.48	74.52 \pm 0.02	73.50 \pm 0.01	21.88 \pm 0.04	21.77 \pm 0.03	14.39 \pm 0.08	22.69 \pm 0.00
	MAPE(%)	16.19	52.10	57.97	58.22	53.01	OOM	50.76	33.07 \pm 0.46	33.89 \pm 0.33	33.89 \pm 1.18	38.46 \pm 0.35	43.75 \pm 1.54	38.90 \pm 0.77	64.65 \pm 0.08	50.35 \pm 0.60	51.52 \pm 0.07	50.81 \pm 0.21	45.00 \pm 1.23	42.32 \pm 0.00
1 st count	MAE	2.38	8.05	10.87	10.94	7.96	OOM	8.56	5.17 \pm 0.19	4.98 \pm 0.16	7.31 \pm 0.41	4.19 \pm 0.04	9.03 \pm 0.25	4.83 \pm 0.27	43.76 \pm 0.00	43.30 \pm 0.20	6.87 \pm 0.03	9.66 \pm 0.01	6.64 \pm 0.12	21.91 \pm 0.00
	Short RMSE	5.29	21.24	24.34	25.32	20.18	OOM	20.82	11.82 \pm 0.36	11.24 \pm 0.29	15.85 \pm 1.04	10.80 \pm 0.09	17.00 \pm 0.36	12.29 \pm 0.30	134.60 \pm 0.00	133.84 \pm 0.10	19.34 \pm 0.06	22.36 \pm 0.01	16.70 \pm 0.19	44.59 \pm 0.00
	MAPE(%)	4.49	10.95	19.56	15.79	11.49	OOM	10.94	21.38 \pm 1.40	14.64 \pm 1.27	14.06 \pm 1.65	10.61 \pm 0.41	34.87 \pm 0.45	14.58 \pm 1.35	61.58 \pm 2.26	49.66 \pm 0.97	10.86 \pm 0.17	17.55 \pm 0.09	12.95 \pm 0.71	26.65 \pm 0.00
1 st count	MAE	12.92	19.84	17.21	23.68	OOM	OOM	22.64	8.37 \pm 0.42	9.30\pm0.09	10.94 \pm 0.61	14.45 \pm 0.37	12.54 \pm 0.05	12.25 \pm 0.04	49.78 \pm 0.02	44.99 \pm 0.29	18.10 \pm 0.05	20.65 \pm 0.04	12.72 \pm 0.00	21.93 \pm 0.00
	Long RMSE	23.54	43.94	38.44	49.65	OOM	OOM	46.92	19.44 \pm 0.71	20.45 \pm 0.14	23.49 \pm 0.79	32.30 \pm 0.65	25.54 \pm 0.21	26.85 \pm 0.45	137.82 \pm 0.01	134.66 \pm 0.15	42.55 \pm 0.13	43.88 \pm 0.08	27.26 \pm 0.00	44.62 \pm 0.00
	MAPE(%)	20.62	24.49	22.70	86.22	OOM	OOM	25.93	15.59 \pm 0.91	21.00 \pm 0.68	23.63 \pm 3.63	23.65 \pm 0.67	41.76 \pm 1.28	24.25 \pm 0.43	73.46 \pm 2.81	55.91 \pm 1.51	24.89 \pm 0.17	31.87 \pm 0.32	24.41 \pm 0.00	26.67 \pm 0.00

Table D.5 Impact of the scale of pre-training datasets on downstream forecasting performance.

Dataset	Metric	Pre-training Data Ratio				
		1	2	4	5	10
PEMS03	MAE	21.87	19.73	18.43	16.78	15.62
	Short RMSE	33.47	30.60	28.28	26.29	23.24
	MAPE(%)	27.67	18.96	19.70	16.35	15.24
PEMS04	MAE	28.52	27.00	24.21	20.55	17.03
	Long RMSE	42.81	40.68	37.07	32.14	26.30
	MAPE(%)	43.53	29.16	26.60	20.29	15.96
PEMS07	MAE	28.37	25.90	24.43	22.85	20.95
	Short RMSE	43.31	40.00	37.95	36.14	32.21
	MAPE(%)	23.11	18.23	17.89	15.64	13.42
PEMS08	MAE	36.78	35.82	32.80	29.15	23.00
	Long RMSE	54.16	53.72	49.82	45.26	35.26
	MAPE(%)	21.75	28.24	25.84	20.63	15.03
PEMS03	MAE	35.19	31.67	29.30	27.13	23.71
	Short RMSE	51.07	46.90	43.33	40.61	34.99
	MAPE(%)	21.75	14.80	14.38	12.97	11.26
PEMS04	MAE	46.10	44.72	40.38	35.36	26.39
	Long RMSE	65.03	64.69	58.91	52.35	38.93
	MAPE(%)	33.35	22.84	20.88	16.90	12.09
PEMS07	MAE	24.40	21.38	19.90	18.60	17.70
	Short RMSE	35.32	31.72	29.86	28.60	25.80
	MAPE(%)	24.29	15.40	15.64	14.61	13.18
PEMS08	MAE	31.02	29.57	26.60	23.27	19.19
	Long RMSE	44.05	43.00	39.46	35.40	28.57
	MAPE(%)	34.02	21.92	20.85	17.54	13.77

Table D.6 Performance comparison with different numbers of spatial and temporal layers in UrbanFM.

Dataset	Metric	Layer Number				
		2	4	6	8	10
PEMS03	MAE	19.73	16.89	15.28	15.62	16.06
	Short RMSE	28.92	26.22	23.79	23.24	25.27
	MAPE(%)	23.01	16.29	15.20	15.24	15.01
PEMS04	MAE	17.87	17.31	17.04	17.03	17.26
	Long RMSE	27.84	26.87	26.51	26.30	26.70
	MAPE(%)	18.61	17.37	17.01	15.96	16.98
PEMS07	MAE	26.14	22.83	20.89	20.95	21.83
	Short RMSE	38.89	36.14	33.11	32.21	34.68
	MAPE(%)	19.87	15.76	14.64	13.42	14.74
PEMS04	MAE	25.45	24.56	24.24	23.00	24.48
	Long RMSE	39.91	38.49	38.08	35.26	38.27

Table D.7 Performance comparison on temporal sizes.

Dataset	Metric	Temporal Window Size				
		24	48	64	128	
PEMS03	Short	MAE	14.84	15.62	18.77	19.79
		RMSE	23.19	23.24	28.93	30.45
		MAPE(%)	14.10	15.24	17.93	20.38
	Long	MAE	23.15	17.03	17.69	25.82
		RMSE	35.75	26.30	27.48	40.28
		MAPE(%)	22.50	15.96	17.79	26.10
PEMS04	Short	MAE	20.80	20.95	24.74	25.97
		RMSE	33.18	32.21	38.99	40.14
		MAPE(%)	14.20	13.42	16.99	18.17
	Long	MAE	31.48	23.00	24.69	33.00
		RMSE	47.25	35.26	38.87	50.39
		MAPE(%)	23.04	15.03	17.57	22.72
PEMS07	Short	MAE	24.05	23.71	30.33	32.25
		RMSE	36.75	34.99	45.11	47.41
		MAPE(%)	10.84	11.26	14.49	16.26
	Long	MAE	38.01	26.39	29.35	41.12
		RMSE	55.61	38.93	43.76	59.82
		MAPE(%)	19.08	12.09	14.26	20.64
PEMS08	Short	MAE	16.53	17.70	22.27	22.63
		RMSE	25.88	25.80	33.26	33.72
		MAPE(%)	11.37	13.18	17.46	19.05
	Long	MAE	26.00	19.19	20.05	28.62
		RMSE	38.50	28.57	30.81	41.91
		MAPE(%)	18.42	13.77	15.50	23.06

Table D.8 Performance comparison on spatial sizes.

Dataset	Metric	Spatial Window Size				
		16	48	64	128	
PEMS03	Short	MAE	15.62	15.86	16.74	17.55
		RMSE	23.24	25.63	27.15	29.27
		MAPE(%)	15.24	15.61	16.93	17.46
	Long	MAE	17.03	16.71	17.44	17.53
		RMSE	26.30	26.68	28.11	28.77
		MAPE(%)	15.96	17.27	18.11	18.04
PEMS04	Short	MAE	20.95	22.65	23.38	20.35
		RMSE	32.21	36.00	37.28	35.24
		MAPE(%)	13.42	15.42	15.88	16.19
	Long	MAE	23.00	24.73	25.37	21.27
		RMSE	35.26	38.70	39.94	36.80
		MAPE(%)	15.03	17.61	18.15	17.73
PEMS07	Short	MAE	23.71	27.31	28.02	29.09
		RMSE	34.99	41.29	42.39	43.97
		MAPE(%)	11.26	13.53	15.03	15.00
	Long	MAE	26.39	29.87	30.52	30.62
		RMSE	38.93	44.53	45.54	45.66
		MAPE(%)	12.09	15.24	15.50	15.91
PEMS08	Short	MAE	17.70	17.44	17.87	13.83
		RMSE	25.80	28.24	28.74	25.53
		MAPE(%)	13.18	16.58	18.45	16.77
	Long	MAE	19.19	18.66	18.72	14.01
		RMSE	28.57	29.98	30.21	26.13
		MAPE(%)	13.77	18.00	17.50	17.14

E.1.1 Privacy and Anonymity.

Although WorldST aggregates data at the flow level to protect anonymity, theoretical re-identification risks persist. We strictly adhere to differential privacy principles during pre-processing to mitigate these risks, ensuring that no single user’s data significantly influences macroscopic patterns.

E.1.2 Fairness in Modeling.

Data coverage is inherently biased towards developed regions with better sensor infrastructure, potentially leading to a “rich-get-richer” performance disparity. We acknowledge this inevitable reality and highlight that addressing such regional fairness remains a critical direction for future research.

E.1.3 Limitations.

Currently, UrbanFM focuses on structured Euclidean Sensor-based and Grid-based data. It does not yet fully integrate unstructured modalities, such as text (*e.g.*, traffic incident reports) or visual feeds (*e.g.*, CCTV footage), which represents a key future avenue for developing truly multi-modal urban foundation models.

E.2 Future Direction

Based on these analyses, we identify three critical avenues for future work to advance urban spatio-temporal foundation models:

E.2.1 Democratizing Urban AI via Few-Shot Transfer.

To mitigate the “rich-get-richer” disparity (Lin et al., 2024) in model performance, future research must focus on data-efficient adaptation techniques. We aim to develop robust few-shot learning or parameter-efficient fine-tuning (PEFT) strategies that allow the foundation model—trained on data-rich metropolises—to be

effectively adapted to underdeveloped regions with sparse sensor infrastructure, thereby promoting global equity in urban intelligence.

E.2.2 Multi-Modal Alignment with LLMs.

Current models are confined to numerical sensor readings. A key frontier is aligning these quantitative spatio-temporal representations with qualitative semantic knowledge from Large Language Models (Liu et al., 2025a,b). Integrating unstructured text (e.g., event descriptions, traffic reports) will enhance the model’s interpretability and reasoning capabilities, enabling it to explain *why* a congestion occurs, not just predict *when*.

E.2.3 From Forecasting to Decision Making.

Forecasting is merely the first step. We envision evolving UrbanFM from a passive predictor into an active *World Model* for urban system. By accurately simulating complex urban dynamics, the foundation model can serve as a simulator for Reinforcement Learning (RL) agents (Wu et al., 2025a), empowering downstream tasks such as traffic signal control and emergency dispatch optimization.